Centroid Moment Tensor catalog with 3D lithospheric wavespeed model: the 2016-2017 Central Apennines sequence

Artale Harris Pietro[1], Scognamiglio Laura[1], Magnoni Federica[1], Casarotti Emanuele[2], and Tinti Elisa[3]

[1]Istituto Nazionale di Geofisica e Vulcanologia
[2]Istituto Nazionale di Geofisica e Vulcanologia. Via di Vigna Murata
[3]Università La Sapienza

November 16, 2022

Abstract

Moment tensor inversions of broadband velocity data are usually managed by adopting Green's functions for 1D layered seismic wavespeed models. This assumption can impact on source parameter estimates in regions with complex 3D heterogeneous structures and rock properties discontinuities. In this work, we present a new Centroid Moment Tensor (CMT) Catalog for the Amatrice–Visso–Norcia (AVN) seismic sequence based on a recently generated 3D wavespeed model for the Italian lithosphere. Forward synthetic seismograms and Fréchet derivatives for CMT–3D inversions of 159 earthquakes with Mw [?] 3.0 are simulated using a spectral–element method (SEM) code. By comparing the retrieved solutions with those from Time Domain Moment Tensor (TDMT) catalog, obtained with a 1D wavespeed model calibrated for Central Apennines (Italy), we observe a remarkable degree of consistency in terms of source geometry, kinematics, and magnitude. Significant differences are found in centroid depths, which are more accurately estimated using the 3D model. Finally, we present a newly designed parameter, τ, to better quantify and compare a–posteriori the reliability of the obtained MT solutions. This parameter measures the goodness of fit between observed and synthetic seismograms accounting for differences in amplitude and arrival time, percentage of fitted seconds, together with the usual L2–norm estimate. These CMT–3D solutions represent the first Italian CMT catalog based on a full–waveform 3D wavespeed model and provide robust source parameters with potential implications for the structures activated during the sequence. The developed approach can be readily applied to more complex Italian regions where a 1D wavespeed model is underperforming.

params_complete

Id	Origin Time	Latitude	Latitude error	Longitude	Longitude error	Depth	Depth error	Mrr	Mrr error	Mtt	Mtt error	Mpp	Mpp error	Mrt	Mrt error	Mrp	Mrp error	Mtp	Mtp error	strike 1	dip 1	rake 1	strike 2	dip 2	rake 2	Magnitude	Magnitude error	Kagan Angle	τ
1	2016/08/24-01:36:32	42.7058	0.0040	13.2474	0.0090	5.90	0.61	-1.06e+25	1.24e+24	2.26e+24	6.50e+23	8.36e+24	1.06e+24	-2.18e+23	5.75e+23	2.47e+24	5.91e+23	-4.53e+24	4.72e+23	326	39	-97	157	51	-83	5.96	0.02	5.70	0.32
2	2016/08/24-02:33:29	42.7959	0.0050	13.1678	0.0110	5.60	0.94	-1.04e+24	1.12e+23	3.83e+23	8.38e+22	6.56e+23	1.11e+23	-1.33e+23	5.85e+22	8.70e+22	5.11e+22	-4.82e+23	3.40e+22	325	40	-85	140	49	-93	5.28	0.02	4.53	0.26
3	2016/08/24-03:08:10	42.6385	0.0530	13.2734	0.0270	6.89	2.96	-5.07e+21	2.32e+21	1.63e+21	2.85e+21	3.44e+21	3.51e+21	1.94e+21	3.09e+21	-2.63e+21	2.27e+21	-1.32e+21	3.44e+21	327	62	-93	155	27	-83	3.77	0.12	7.67	0.42
4	2016/08/24-03:17:59	42.7720	0.0130	13.1617	0.0380	5.36	3.11	-2.79e+21	1.62e+21	-3.83e+20	1.06e+21	3.17e+21	1.43e+21	6.01e+20	1.05e+21	-2.43e+21	2.51e+21	6.16e+19	9.83e+20	350	65	-99	192	26	-70	3.66	0.13	5.06	3.36
5	2016/08/24-03:40:11	42.6251	0.0080	13.2454	0.0270	9.29	1.97	-1.05e+22	3.01e+21	1.74e+21	1.46e+21	8.74e+21	2.80e+21	3.42e+21	2.00e+21	-6.83e+21	2.44e+21	-1.05e+22	3.16e+21	131	31	-108	332	60	-79	4.08	0.05	9.90	0.29
6	2016/08/24-04:06:50	42.7815	0.0100	13.1334	0.0180	3.67	1.32	-3.28e+22	5.40e+21	3.00e+21	4.61e+21	2.98e+22	4.74e+21	-8.79e+21	4.25e+21	-2.49e+21	5.22e+21	-2.00e+22	4.28e+21	348	46	-65	135	49	-113	4.33	0.03	12.55	0.25
7	2016/08/24-04:25:58	42.6513	0.0130	13.2363	0.0170	8.39	2.13	-1.67e+21	4.77e+20	-1.12e+20	2.84e+20	1.79e+21	5.39e+20	1.84e+20	3.14e+20	-9.73e+20	2.54e+20	-4.12e+20	3.90e+20	348	59	-89	167	30	-91	3.48	0.05	6.00	0.37
8	2016/08/24-04:33:09	42.6444	0.0120	13.2272	0.0200	6.22	1.42	-1.45e+21	3.20e+20	5.09e+20	2.40e+20	9.43e+20	2.90e+20	1.14e+20	2.09e+20	-2.59e+20	3.06e+20	-7.36e+20	2.72e+20	325	50	-86	140	39	-93	3.39	0.05	6.12	0.37
9	2016/08/24-04:38:09	42.6304	0.0840	13.2357	0.0250	6.75	3.96	-9.49e+20	1.59e+21	-1.74e+20	2.93e+21	1.12e+21	4.35e+21	5.17e+20	2.86e+21	-4.53e+20	2.28e+21	-4.78e+20	1.24e+21	183	35	-54	322	62	-112	3.35	0.51	16.77	7.9
10	2016/08/24-04:44:38	42.7547	0.0200	13.1905	0.0150	6.08	2.45	-1.94e+21	3.85e+20	8.65e+20	4.46e+20	1.08e+21	6.88e+20	2.48e+20	4.41e+20	8.01e+20	3.18e+20	-1.01e+21	2.43e+20	301	41	-117	155	54	-67	3.49	0.04	4.00	7.81
11	2016/08/24-04:57:37	42.8439	0.0500	13.0558	0.1610	-0.24	2.89	-2.68e+21	1.14e+21	1.81e+21	6.03e+20	8.76e+20	5.38e+20	-4.44e+20	1.10e+21	-2.46e+20	1.45e+21	-1.13e+21	1.50e+21	312	43	-76	114	48	-101	3.55	0.10	7.43	8.87
12	2016/08/24-05:31:31	42.6760	0.0150	13.2105	0.0060	5.85	1.83	-8.13e+20	1.91e+20	-1.15e+20	2.88e+20	9.28e+20	3.57e+20	9.79e+19	1.93e+20	4.96e+20	1.36e+20	-2.78e+20	1.84e+20	329	33	-115	179	60	-73	3.28	0.05	7.89	0.33
13	2016/08/24-05:36:18	42.8079	0.0230	13.1652	0.0150	5.00	3.03	-1.85e+20	3.06e+20	-3.29e+20	4.32e+20	5.15e+20	5.62e+20	5.39e+20	3.71e+20	-8.01e+20	2.63e+20	2.74e+20	3.20e+20	332	85	-117	233	28	-10	3.30	0.08	7.29	0.38
14	2016/08/24-06:54:54	42.7920	0.0200	13.1490	0.0110	4.50	2.56	-3.40e+20	2.60e+20	-2.57e+20	1.74e+20	5.97e+20	2.28e+20	4.99e+20	1.57e+20	-2.62e+20	1.87e+20	-2.89e+19	2.15e+20	209	40	-26	320	72	-127	3.19	0.06	15.37	0.4
15	2016/08/24-09:31:43	42.8195	0.0160	13.1771	0.0120	14.12	2.34	-2.10e+20	2.83e+20	-1.43e+21	4.87e+20	1.64e+21	6.35e+20	4.65e+20	3.33e+20	4.13e+20	2.55e+20	5.03e+20	4.43e+20	324	68	-177	233	88	-21	3.43	0.07	4.35	0.34
16	2016/08/24-11:50:30	42.8332	0.0190	13.1558	0.0160	7.56	1.68	-6.13e+22	1.56e+22	2.82e+22	9.16e+21	3.31e+22	1.14e+22	1.91e+22	7.44e+21	-2.98e+22	1.07e+22	-4.12e+22	7.73e+21	129	31	-100	322	59	-83	4.52	0.04	3.74	0.29
17	2016/08/24-14:02:20	42.8021	0.0160	13.2530	0.0050	2.04	1.56	-2.37e+21	1.12e+21	-1.31e+21	1.04e+21	3.68e+21	1.58e+21	1.27e+21	1.26e+21	-1.11e+20	7.55e+20	3.53e+20	8.07e+20	334	54	-133	213	53	-46	3.63	0.09	7.58	0.36
18	2016/08/24-17:46:09	42.6716	0.0090	13.2276	0.0080	8.71	0.74	-2.18e+22	2.28e+21	2.86e+20	2.09e+21	2.15e+22	2.09e+21	1.16e+21	2.33e+21	-8.69e+21	1.35e+21	-8.62e+21	2.44e+21	345	55	-84	155	35	-98	4.20	0.02	6.10	0.25
19	2016/08/24-20:21:35	42.7890	0.0120	13.1579	0.0090	4.57	1.56	-5.52e+20	2.64e+20	-3.35e+19	1.29e+20	5.86e+20	3.04e+20	5.11e+20	1.17e+20	-2.11e+20	9.88e+19	-2.93e+20	1.82e+20	183	35	-42	311	66	-117	3.22	0.06	12.34	0.36
20	2016/08/24-23:22:05	42.6521	0.0080	13.2155	0.0090	8.42	1.24	-9.42e+21	1.19e+21	-3.72e+19	8.10e+20	9.46e+21	1.10e+21	3.23e+21	1.01e+21	-6.07e+21	9.65e+20	-4.25e+21	7.17e+20	164	28	-81	334	61	-94	4.00	0.02	4.27	0.33
21	2016/08/25-03:17:16	42.7638	0.0120	13.2096	0.0120	7.01	0.94	-2.51e+22	3.96e+21	-2.29e+21	4.42e+21	2.74e+22	4.98e+21	8.42e+21	2.73e+21	-1.64e+22	4.09e+21	-2.43e+21	2.84e+21	342	62	-103	189	30	-66	4.28	0.03	3.76	0.28
22	2016/08/25-04:12:11	42.6951	0.0040	13.2337	0.0080	5.91	1.46	-6.36e+20	2.04e+20	-8.32e+19	1.22e+20	7.20e+20	1.98e+20	1.10e+20	1.37e+20	1.11e+20	9.57e+19	-4.65e+19	8.25e+19	345	41	-106	187	50	-75	3.17	0.06	7.63	0.37
23	2016/08/25-04:51:40	42.6279	0.0120	13.3338	0.0110	1.29	1.22	-4.23e+21	1.06e+21	1.76e+21	6.38e+20	2.47e+21	9.13e+20	-1.75e+21	8.45e+20	2.15e+21	6.96e+20	-1.52e+21	5.09e+20	321	27	-89	141	62	-90	3.73	0.04	3.46	0.35
24	2016/08/25-12:36:05	42.5943	0.0120	13.3083	0.0220	4.97	2.47	-2.93e+22	8.88e+21	6.72e+21	3.88e+21	2.26e+22	7.71e+21	-2.31e+22	5.35e+21	6.21e+20	6.23e+21	-3.03e+22	4.76e+21	352	43	-40	113	63	-126	4.38	0.03	16.14	0.28
25	2016/08/25-19:40:44	42.5919	0.0250	13.2759	0.0230	5.47	1.54	-1.30e+21	3.97e+20	2.93e+20	3.37e+20	1.00e+21	3.45e+20	-5.44e+20	5.45e+20	-2.68e+20	4.32e+20	-1.03e+21	3.00e+20	349	49	-52	120	52	-125	3.42	0.06	9.54	0.39
26	2016/08/26-00:04:09	42.6819	0.0170	13.2830	0.0090	1.47	1.64	-1.79e+21	4.57e+20	5.37e+20	3.08e+20	1.25e+21	4.80e+20	-5.25e+20	3.53e+20	7.62e+20	3.67e+20	-1.11e+21	2.87e+20	144	57	-89	323	32	-91	3.49	0.04	8.84	0.33
27	2016/08/26-04:28:25	42.5988	0.0110	13.3121	0.0190	4.28	1.37	-8.27e+22	3.12e+22	3.12e+22	1.38e+22	5.15e+22	2.02e+22	-6.02e+22	1.54e+22	9.84e+21	1.63e+22	-9.80e+22	1.70e+22	111	63	-125	349	42	-40	4.69	0.04	20.18	0.24
28	2016/08/26-05:17:05	42.7546	0.0090	13.2148	0.0410	6.26	2.24	4.32e+20	2.21e+20	-6.28e+20	2.86e+20	1.96e+20	3.64e+20	5.02e+20	1.92e+20	-5.87e+20	2.13e+20	2.76e+20	2.93e+20	134	74	114	254	28	32	3.27	0.06	17.47	0.45
29	2016/08/26-05:32:52	42.7739	0.0140	13.1564	0.0070	2.35	3.01	-4.42e+20	2.10e+20	-1.37e+20	1.75e+20	5.79e+20	2.28e+20	5.53e+20	2.48e+20	-8.42e+20	1.82e+20	6.05e+19	1.88e+20	332	78	-107	210	20	-33	3.31	0.05	18.97	0.37
30	2016/08/26-16:05:29	42.7019	0.0070	13.1455	0.0050	7.63	1.63	-1.57e+21	2.02e+20	6.59e+20	2.44e+20	9.10e+20	2.77e+20	1.02e+21	2.52e+20	-7.98e+20	1.54e+20	-8.48e+20	1.62e+20	312	64	-96	146	26	-76	3.48	0.03	7.50	0.35
31	2016/08/27-01:26:39	42.8446	0.0150	13.2461	0.0110	1.06	2.86	-3.63e+21	1.50e+21	-1.34e+20	9.67e+20	3.76e+21	1.41e+21	-3.55e+20	1.22e+21	1.41e+21	1.02e+21	-2.88e+21	1.25e+21	159	54	-79	322	36	-104	3.73	0.07	3.00	0.37
32	2016/08/27-02:50:59	42.8531	0.0140	13.2477	0.0160	1.87	1.80	-4.60e+21	2.53e+21	-1.32e+21	1.95e+21	5.92e+21	1.55e+21	-1.71e+21	9.07e+20	4.31e+21	9.55e+20	-4.90e+21	1.07e+21	161	63	-80	319	28	-108	3.89	0.04	11.37	0.24
33	2016/08/27-06:20:30	42.5483	0.0120	13.3246	0.0340	2.26	1.80	-8.17e+20	1.98e+20	5.46e+20	2.01e+20	2.72e+20	2.69e+20	-1.56e+20	2.43e+20	-4.41e+20	1.87e+20	-5.59e+20	1.90e+20	332	55	-57	104	46	-128	3.28	0.05	9.75	0.36
34	2016/08/27-10:40:14	42.8607	0.0190	13.2539	0.0100	-0.56	2.91	-1.39e+21	8.45e+20	-7.77e+19	4.44e+20	1.47e+21	6.82e+20	-4.20e+20	6.85e+20	1.26e+21	4.09e+20	-1.37e+21	6.23e+20	162	64	-74	310	29	-118	3.52	0.07	14.17	0.37
35	2016/08/28-06:37:19	42.7309	0.0070	13.2098	0.0070	9.12	1.21	-1.09e+21	1.95e+20	1.93e+20	1.12e+20	8.95e+20	1.86e+20	4.11e+20	8.60e+19	-3.84e+20	9.06e+19	-5.02e+20	8.63e+19	323	58	-99	161	33	-74	3.34	0.03	4.66	0.35
36	2016/08/28-13:07:32	42.6250	0.0250	13.2897	0.0070	3.33	2.68	-1.43e+21	3.55e+20	-3.43e+20	2.88e+20	1.78e+21	2.56e+20	-8.12e+20	3.54e+20	1.40e+21	3.88e+20	-7.39e+20	4.61e+20	151	67	-101	358	25	-64	3.53	0.04	7.59	0.36
37	2016/08/28-15:37:38	42.7713	0.0070	13.1151	0.0090	9.34	1.53	-1.89e+21	1.99e+20	-2.29e+20	1.72e+20	2.12e+21	2.27e+20	6.09e+19	1.43e+20	-4.97e+20	1.28e+20	-8.50e+20	1.77e+20	158	38	-95	345	51	-85	3.50	0.02	5.44	0.35
38	2016/08/28-15:55:35	42.7976	0.0210	13.2461	0.0110	6.20	0.60	-1.17e+22	5.85e+21	6.34e+21	3.89e+21	5.41e+21	9.17e+21	5.63e+21	1.65e+21	4.47e+21	1.26e+21	8.91e+21	2.45e+21	42	30	-96	229	59	-86	4.06	0.06	22.82	0.27
39	2016/08/28-16:42:01	42.8267	0.0090	13.1431	0.0060	2.34	1.41	-3.51e+21	6.05e+20	5.42e+19	3.39e+20	3.46e+21	5.39e+20	3.77e+20	5.23e+20	-9.95e+20	3.88e+20	-1.81e+21	5.05e+20	155	37	-91	337	52	-88	3.68	0.03	2.50	0.35
40	2016/08/29-01:44:25	42.7733	0.0080	13.1838	0.0140	5.54	2.57	-8.30e+20	2.66e+20	3.48e+20	2.11e+20	4.82e+20	2.96e+20	-4.09e+20	1.77e+20	-2.93e+19	1.64e+20	-5.29e+20	2.14e+20	338	40	-58	119	56	-114	3.27	0.06	10.58	0.35
41	2016/08/30-00:35:55	42.8032	0.0250	13.1365	0.0190	8.30	3.31	-9.99e+20	3.03e+20	3.42e+20	3.19e+20	6.57e+20	3.48e+20	-1.38e+20	3.08e+20	-4.72e+20	1.82e+20	-8.74e+20	3.14e+20	343	56	-58	115	44	-128	3.35	0.06	7.64	0.32
42	2016/08/31-11:26:01	42.8418	0.0030	13.1434	0.0070	4.72	0.66	-6.31e+21	9.96e+20	2.72e+20	5.45e+20	6.04e+21	8.80e+20	9.74e+20	9.67e+20	-3.36e+21	6.89e+20	-2.56e+21	9.38e+20	341	58	-87	156	31	-94	3.86	0.03	6.77	0.38
43	2016/08/31-11:52:31	42.8738	0.0100	13.2517	0.0230	0.44	2.69	1.21e+20	2.81e+20	-4.41e+20	3.77e+20	3.20e+20	3.16e+20	1.71e+20	5.52e+20	7.64e+18	2.36e+20	-1.07e+21	4.73e+20	279	89	-171	189	81	0	3.31	0.11	6.42	0.37
44	2016/08/31-13:23:04	42.7683	0.0200	13.2478	0.0080	4.91	2.40	-6.59e+20	1.83e+20	2.83e+20	2.12e+20	3.76e+20	2.52e+20	-3.21e+20	1.87e+20	8.25e+20	1.18e+20	-6.01e+20	2.60e+20	155	70	-72	292	25	-129	3.33	0.04	7.00	0.36
45	2016/08/31-18:12:52	42.8324	0.0080	13.2576	0.0280	7.01	1.86	3.93e+19	3.11e+20	-1.81e+21	4.29e+20	1.78e+21	5.70e+20	3.94e+20	2.25e+20	-4.63e+20	2.25e+20	3.01e+20	2.98e+20	229	71	0	139	89	161	3.46	0.05	8.13	0.37
46	2016/09/01-03:53:03	42.6280	0.0060	13.3166	0.0230	5.99	1.55	-1.96e+21	3.96e+20	9.24e+20	2.48e+20	1.04e+21	3.99e+20	-1.07e+21	2.76e+20	1.45e+21	3.41e+20	-1.55e+21	2.71e+20	141	64	-83	308	26	-102	3.58	0.03	9.11	0.39
47	2016/09/01-11:35:57	42.5708	0.0120	13.3267	0.0210	4.74	1.13	-2.64e+20	3.18e+20	-8.35e+19	3.93e+20	3.47e+20	3.72e+20	7.75e+20	2.19e+20	-1.23e+20	3.18e+20	-5.42e+20	2.98e+20	183	36	-15	286	80	-125	3.27	0.07	3.99	0.42
48	2016/09/03-01:34:12	42.7850	0.0130	13.1476	0.0120	3.68	1.31	-2.06e+22	3.54e+21	-3.74e+20	2.89e+21	2.10e+22	3.07e+21	2.74e+21	3.31e+21	-1.46e+21	2.68e+21	-4.62e+21	2.43e+21	341	48	-99	175	42	-79	4.16	0.03	6.06	0.25
49	2016/09/03-10:18:51	42.8849	0.0120	13.2262	0.0100	7.11	1.86	-3.38e+21	5.67e+21	-2.44e+22	6.67e+21	2.78e+22	4.14e+21	2.13e+21	2.07e+21	2.29e+21	3.21e+21	-2.02e+22	5.64e+21	296	84	-177	205	87	-5	4.28	0.04	7.26	0.25
50	2016/09/07-18:13:26	42.8407	0.0240	13.2602	0.0210	0.27	2.16	-6.74e+20	2.88e+20	3.06e+20	2.54e+20	3.68e+20	2.44e+20	-2.15e+20	2.85e+20	6.92e+19	4.94e+20	-6.07e+20	1.42e+20	124	53	-106	330	39	-69	3.23	0.06	13.09	0.4
51	2016/09/15-14:40:52	42.7873	0.0170	13.1450	0.0060	-0.31	1.58	-2.37e+21	9.25e+20	3.77e+19	6.09e+20	2.33e+21	9.31e+20	1.51e+21	5.61e+20	-1.40e+21	5.13e+20	1.36e+20	4.30e+20	201	33	-50	336	65	-112	3.60	0.06	18.83	0.34
52	2016/09/19-23:34:25	42.6910	0.0130	13.2806	0.0070	1.31	1.64	-2.30e+21	5.87e+20	1.80e+21	1.23e+21	5.06e+20	8.64e+20	1.39e+21	5.54e+20	-2.51e+21	5.21e+20	-1.13e+21	3.91e+20	322	71	-74	101	24	-128	3.65	0.04	25.08	0.34
53	2016/09/20-01:20:53	42.6873	0.0870	13.2914	0.0240	6.02	2.07	-2.07e+20	1.08e+21	5.81e+20	1.76e+21	-3.75e+20	1.13e+21	4.83e+20	7.05e+20	-6.86e+20	6.13e+20	-9.60e+19	8.78e+20	317	83	-59	58	30	-166	3.27	0.23	11.25	7.08
54	2016/09/22-20:03:54	42.7204	0.0730	13.1865	0.0150	1.15	2.81	-7.62e+20	1.12e+21	4.63e+20	8.38e+20	2.98e+20	1.41e+21	1.74e+20	8.57e+20	-7.56e+20	2.21e+20	-6.89e+20	5.79e+20	104	34	-136	335	67	-64	3.33	0.13	11.30	0.4
55	2016/09/30-19:22:28	42.8748	0.0310	13.2558	0.0200	1.46	3.16	-3.84e+20	4.61e+20	-3.49e+20	4.10e+20	7.34e+20	3.46e+20	-1.10e+20	3.49e+20	3.77e+20	1.15e+20	-5.37e+20	4.17e+20	291	63	-174	198	85	-26	3.25	0.10	47.23	0.31
56	2016/09/30-19:38:37	42.8722	0.0400	13.2562	0.0300	2.03	3.09	-1.53e+21	4.15e+20	-2.45e+20	4.69e+20	1.77e+21	6.23e+20	-5.28e+20	6.04e+20	3.38e+20	2.27e+20	-9.70e+20	4.34e+20	141	55	-112	357	40	-61	3.47	0.06	43.80	0.34
57	2016/10/02-23:47:07	42.8174	0.2720	13.2483	0.0060	-4.57	6.41	7.55e+20	1.56e+21	-3.99e+20	1.30e+21	-3.56e+20	2.97e+20	1.31e+18	2.13e+20	7.06e+19	3.18e+20	-2.38e+20	3.32e+20	44	47	85	230	43	94	3.17	0.39	112.96	6.18
58	2016/10/04-12:41:35	42.8637	0.0900	13.1142	0.0550	7.25	4.46	-1.39e+21	1.37e+21	5.85e+20	1.30e+21	8.01e+20	1.24e+21	-7.38e+20	1.88e+21	-6.20e+20	5.66e+20	-1.45e+21	5.02e+20	347	54	-43	106	55	-135	3.49	0.13	2.76	6.35
59	2016/10/08-12:19:03	42.7787	0.0320	13.1444	0.0200	4.56	2.91	-2.47e+21	6.81e+20	7.14e+20	4.62e+20	1.75e+21	9.03e+20	-3.59e+20	7.36e+20	-5.38e+20	3.86e+20	-1.14e+21	3.48e+20	339	49	-73	134	43	-108	3.54	0.06	9.92	0.36
60	2016/10/08-18:11:09	42.7427	0.0130	13.1954	0.0090	2.29	2.45	-7.64e+21	2.50e+21	1.24e+21	1.37e+21	6.41e+21	2.00e+21	-7.17e+20	1.59e+21	4.36e+20	1.13e+21	-4.81e+21	1.32e+21	332	42	-84	145	47	-94	3.89	0.05	9.76	0.36
61	2016/10/16-09:32:35	42.7625	0.0130	13.2113	0.0110	1.28	1.12	-9.06e+21	8.82e+20	-2.44e+20	1.22e+21	9.31e+21	1.32e+21	1.28e+21	1.74e+21	-3.17e+19	2.12e+21	-3.25e+21	1.30e+21	334	46	-101	171	44	-77	3.93	0.03	9.58	0.24
62	2016/10/26-17:10:36	42.8774	0.0060	13.1437	0.0070	6.15	0.98	-1.09e+24	8.14e+22	4.88e+22	7.78e+22	1.04e+24	9.22e+22	1.86e+23	5.65e+22	-3.27e+23	1.05e+23	-3.82e+23	6.54e+22	337	54	-94	165	36	-83	5.32	0.02	4.13	0.23
63	2016/10/26-19:18:08	42.9180	0.0100	13.1045	0.0080	4.55	0.50	-7.35e+24	7.80e+23	8.81e+23	4.88e+23	6.47e+24	5.82e+23	1.83e+23	3.00e+23	2.30e+24	7.09e+23	-2.50e+24	2.10e+23	166	53	-81	331	37	-101	5.86	0.02	8.57	0.29
64	2016/10/26-21:42:01	42.8676	0.0070	13.1380	0.0130	5.25	1.44	-5.34e+22	4.53e+21	5.12e+21	4.19e+21	4.83e+22	5.03e+21	1.58e+22	6.27e+21	-1.53e+22	5.21e+21	-2.12e+22	3.76e+21	328	55	-100	166	35	-75	4.45	0.02	8.02	0.23
65	2016/10/27-03:19:27	42.8567	0.0330	13.1741	0.0190	3.32	3.47	-7.87e+21	5.05e+21	-1.07e+21	3.48e+21	8.94e+21	3.23e+21	3.15e+21	1.78e+21	-7.12e+20	1.94e+21	-3.61e+21	1.91e+21	321	54	-117	183	43	-57	3.93	0.08	22.14	0.27
66	2016/10/27-03:50:24	43.0139	0.0310	13.1126	0.0170	8.00	4.05	-1.17e+22	8.02e+21	-7.03e+20	5.99e+21	1.24e+22	5.07e+21	-4.22e+21	4.99e+21	-1.02e+22	3.20e+21	-5.02e+21	3.02e+21	137	33	-132	5	66	-65	4.09	0.07	13.23	0.26
67	2016/10/27-08:21:45	42.8803	0.0150	13.1204	0.0110	4.42	0.87	-2.69e+22	3.10e+21	-3.51e+21	3.37e+21	3.04e+22	3.57e+21	8.20e+21	5.09e+21	-2.04e+22	3.21e+21	-3.98e+21	2.87e+21	184	27	-70	343	63	-99	4.31	0.02	7.25	0.25
68	2016/10/27-17:22:23	42.8385	0.0210	13.1150	0.0070	5.04	0.96	-1.96e+22	4.28e+21	-3.33e+21	4.07e+21	2.29e+22	2.78e+21	-1.27e+21	6.29e+21	-1.68e+22	3.65e+21	1.51e+21	2.57e+21	3	64	-89	182	25	-91	4.23	0.03	2.34	0.27
69	2016/10/29-16:24:33	42.8406	0.0140	13.1113	0.0110	9.86	1.29	-1.80e+22	3.23e+21	3.47e+21	1.52e+21	1.45e+22	2.87e+21	3.29e+21	1.11e+21	-5.05e+20	1.63e+21	-7.18e+21	1.77e+21	325	48	-101	162	42	-77	4.11	0.03	6.31	0.25
70	2016/10/30-06:40:17	42.8392	0.0120	13.1300	0.0070	5.05	0.52	-5.52e+25	6.20e+24	1.07e+25	4.64e+24	4.45e+25	4.15e+24	3.95e+24	4.82e+24	6.95e+24	2.83e+24	-1.95e+25	3.57e+24	329	42	-99	161	47	-81	6.43	0.02	8.06	0.32
71	2016/10/30-10:19:26	42.8488	0.1560	13.1549	0.0080	4.24	5.58	-2.67e+20	3.83e+21	-3.57e+21	7.95e+21	3.84e+21	5.75e+21	-3.21e+21	1.38e+22	2.93e+21	1.72e+22	-1.04e+21	9.66e+21	37	41	-1	129	88	-131	3.78	0.60	36.38	8.0
72	2016/10/30-10:50:37	42.8443	0.0400	13.0857	0.0070	4.29	2.68	-2.07e+21	6.38e+20	2.06e+20	4.67e+20	1.87e+21	7.21e+20	-3.43e+20	1.09e+21	-3.75e+21	3.77e+20	4.52e+20	6.97e+20	200	14	-75	6	75	-93	3.69	0.03	15.20	0.37
73	2016/10/30-11:21:08	43.0572	0.0200	13.0943	0.0130	7.92	3.37	-6.88e+21	3.69e+21	2.92e+21	2.67e+21	3.95e+21	3.43e+21	-3.20e+20	1.78e+21	3.85e+21	1.26e+21	-6.10e+21	1.80e+21	157	58	-64	294	39	-125	3.92	0.06	9.83	0.26
74	2016/10/30-11:58:17	42.8316	0.0240	13.0603	0.0200	15.45	1.95	-4.96e+21	1.61e+21	2.78e+21	2.35e+21	2.18e+21	1.98e+21	5.41e+21	2.58e+21	-1.42e+22	1.93e+21	-1.23e+21	2.29e+21	337	82	-85	128	8	-118	4.07	0.04	6.11	0.23
75	2016/10/30-12:07:00	42.8509	0.0070	13.0876	0.0100	12.20	1.42	-4.09e+22	6.18e+21	4.75e+21	3.41e+21	3.61e+22	5.04e+21	1.76e+22	5.37e+21	-3.66e+22	4.52e+21	-1.60e+22	3.32e+21	335	67	-91	159	22	-85	4.45	0.02	9.22	0.26
76	2016/10/30-13:34:54	42.7994	0.0130	13.1948	0.0140	6.03	1.53	-7.41e+21	2.70e+21	9.08e+21	2.30e+21	-1.67e+21	1.75e+21	-4.07e+21	1.90e+21	9.65e+21	1.05e+21	-8.63e+21	1.02e+21	149	72	-55	263	38	-150	4.07	0.02	3.62	0.24
77	2016/10/30-14:24:44	42.7610	0.0130	13.0660	0.0210	10.37	3.53	-6.74e+20	2.63e+20	3.40e+20	3.85e+20	3.34e+20	4.44e+20	-1.13e+20	3.17e+20	-1.35e+21	3.15e+20	2.96e+20	4.32e+20	236	16	-45	10	78	-101	3.39	0.06	11.63	0.36
78	2016/10/30-18:21:09	42.8084	0.0080	13.1736	0.0040	0.65	0.49	-8.43e+21	6.12e+20	1.53e+21	5.66e+20	6.90e+21	5.68e+20	2.14e+21	8.86e+20	1.01e+20	6.11e+20	-8.94e+20	4.33e+20	339	47	-106	182	45	-73	3.88	0.02	9.59	0.27
79	2016/10/31-03:27:40	42.7653	0.0150	13.0982	0.0180	13.40	2.07	-5.56e+21	1.64e+21	2.81e+21	1.45e+21	2.75e+21	1.90e+21	3.71e+21	1.57e+21	-1.17e+22	1.15e+21	2.54e+21	2.10e+21	349	81	-101	222	14	-37	4.02	0.03	12.71	0.23
80	2016/10/31-07:05:44	42.8474	0.0050	13.1315	0.0090	6.74	1.03	-8.19e+21	1.14e+21	4.06e+20	9.74e+20	7.78e+21	1.30e+21	1.08e+21	1.08e+21	-9.14e+21	1.15e+21	-1.13e+20	1.13e+21	354	69	-92	182	20	-82	3.99	0.02	5.67	0.24
81	2016/10/31-08:40:35	42.8325	0.0210	13.1344	0.0110	2.41	2.50	-1.05e+21	3.40e+20	8.40e+19	2.85e+20	9.62e+20	3.53e+20	2.82e+20	2.24e+20	-7.04e+20	2.73e+20	-4.79e+20	4.42e+20	337	62	-88	154	27	-92	3.36	0.06	5.73	0.37
82	2016/11/01-07:56:39	43.0220	0.0100	13.1566	0.0180	4.89	1.30	-1.52e+23	4.50e+22	7.02e+21	3.03e+22	1.45e+23	2.92e+22	1.78e+22	1.17e+22	3.25e+22	1.57e+22	-8.07e+22	1.71e+22	322	42	-109	167	50	-73	4.76	0.04	8.30	0.23
83	2016/11/02-19:37:49	42.8799	0.0220	13.0771	0.0080	1.19	1.48	-2.71e+21	8.05e+20	7.30e+20	4.36e+20	1.98e+21	8.80e+20	7.64e+20	6.05e+20	-9.62e+19	4.86e+20	-1.99e+21	3.81e+20	310	51	-108	158	41	-68	3.61	0.05	13.85	0.37
84	2016/11/03-00:35:01	43.0243	0.0100	13.0590	0.0110	6.25	1.21	-8.23e+22	9.47e+21	1.38e+21	8.70e+21	8.09e+22	1.08e+22	5.32e+22	1.38e+22	-7.91e+22	1.11e+22	-3.42e+22	1.24e+22	171	22	-68	329	68	-98	4.68	0.02	4.24	0.25
85	2016/11/03-10:14:13	42.8110	0.0580	13.2070	0.0350	2.35	4.29	-3.31e+20	1.35e+20	1.78e+20	1.60e+20	1.53e+20	1.61e+20	5.45e+19	1.30e+20	-1.70e+20	1.82e+20	4.47e+18	1.85e+20	337	63	-87	153	26	-94	2.96	0.11	32.15	0.36
86	2016/11/05-11:05:45	42.9816	0.0150	13.1956	0.0470	-0.20	2.22	-1.10e+21	8.75e+20	5.57e+20	1.47e+21	5.38e+20	1.81e+21	-8.65e+20	3.85e+20	1.31e+21	1.43e+21	-4.43e+20	1.43e+21	307	17	-106	144	73	-85	3.45	0.18	31.17	0.37
87	2016/11/07-18:56:16	42.8896	0.0050	13.1524	0.0070	9.37	1.03	-6.26e+21	8.54e+20	1.07e+20	6.03e+20	6.15e+21	9.26e+20	2.74e+21	6.04e+20	-2.11e+21	4.76e+20	-2.35e+21	9.67e+20	325	58	-107	176	35	-63	3.85	0.03	1.31	0.34
88	2016/11/12-14:43:33	42.7359	0.0190	13.2263	0.0130	4.87	1.57	-1.27e+22	2.92e+21	1.88e+20	2.97e+21	1.25e+22	2.63e+21	3.89e+21	2.05e+21	-2.17e+21	2.19e+21	-8.00e+21	2.56e+21	168	39	-68	320	53	-107	4.07	0.04	10.09	0.23
89	2016/11/12-22:32:23	42.8247	0.0190	13.1446	0.0090	5.09	1.40	-1.75e+21	5.32e+20	-4.72e+18	3.15e+20	1.75e+21	5.81e+20	1.47e+20	2.67e+20	3.53e+20	2.32e+20	-1.81e+20	3.72e+20	179	50	-82	348	39	-98	3.44	0.06	1.86	0.37
90	2016/11/16-11:52:22	42.8062	0.0100	13.1413	0.0090	8.40	2.38	-1.52e+21	1.23e+21	3.45e+21	1.24e+21	-1.93e+21	1.60e+21	-3.54e+21	1.29e+21	4.13e+21	1.10e+21	1.61e+21	1.69e+21	223	32	-166	121	82	-57	3.81	0.05	14.69	0.37
91	2016/11/27-21:41:14	43.0220	0.0060	13.0805	0.0100	3.95	1.57	-5.73e+21	1.72e+21	1.30e+21	1.83e+21	4.42e+21	1.08e+21	-1.37e+21	1.17e+21	3.21e+20	7.27e+20	-3.40e+21	1.19e+21	338	41	-73	136	50	-103	3.81	0.05	11.91	0.37
92	2016/11/29-16:14:02	42.5308	0.0060	13.3099	0.0110	8.86	1.20	-2.28e+22	2.71e+21	-4.72e+20	2.30e+21	2.33e+22	3.29e+21	2.10e+22	3.47e+21	-3.53e+22	3.67e+21	-1.26e+22	2.08e+21	166	16	-73	329	74	-94	4.40	0.02	8.31	0.27
93	2016/12/01-11:30:53	43.0047	0.0020	13.0895	0.0070	2.69	0.97	-6.45e+21	1.33e+21	-2.86e+20	1.71e+21	6.74e+21	1.41e+21	1.49e+21	1.37e+21	-1.34e+21	7.02e+20	-3.42e+21	1.06e+21	168	38	-74	328	52	-101	3.86	0.04	6.35	0.39
94	2017/01/02-03:36:13	42.8149	0.0050	12.7604	0.0160	4.05	2.48	1.03e+21	1.01e+21	4.53e+21	1.76e+21	-5.56e+21	1.56e+21	1.48e+21	1.22e+21	-2.45e+21	1.35e+21	-6.67e+21	2.04e+21	162	83	19	70	70	173	3.90	0.06	10.44	0.43
95	2017/01/18-09:25:40	42.5473	0.0050	13.2796	0.0080	6.78	1.00	-4.49e+23	5.27e+22	4.61e+22	3.67e+22	4.03e+23	4.25e+22	2.21e+23	4.43e+22	-3.07e+23	3.88e+22	-2.38e+23	4.98e+22	161	26	-77	327	64	-96	5.13	0.02	6.94	0.25
96	2017/01/18-10:14:09	42.5314	0.0040	13.3053	0.0090	4.74	0.79	-1.66e+24	1.41e+23	-5.29e+22	1.18e+23	1.71e+24	1.62e+23	-3.73e+22	1.30e+23	5.60e+23	1.16e+23	-7.04e+23	1.58e+23	334	36	-99	166	53	-82	5.46	0.02	4.42	0.25
97	2017/01/18-10:25:23	42.4970	0.0070	13.3276	0.0090	8.00	1.32	-1.11e+24	9.82e+22	3.81e+23	7.12e+22	7.26e+23	7.57e+22	4.02e+23	7.66e+22	-3.84e+23	8.99e+22	-7.13e+23	7.78e+22	146	32	-82	317	57	-94	5.35	0.02	4.57	0.29
98	2017/01/18-11:07:37	42.6152	0.0280	13.2749	0.0120	8.47	2.67	-1.35e+22	5.45e+21	3.53e+21	8.89e+21	9.93e+21	1.09e+22	6.38e+21	4.02e+21	-4.93e+21	5.10e+21	-8.72e+21	7.51e+21	156	32	-72	315	59	-100	4.09	0.10	7.56	0.29
99	2017/01/18-13:33:36	42.4792	0.0060	13.2874	0.0110	8.50	0.95	-1.53e+23	2.43e+22	-6.02e+22	2.24e+22	2.14e+23	2.32e+22	2.51e+23	2.46e+22	-1.96e+23	2.14e+22	-1.42e+23	2.07e+22	191	27	-31	309	76	-113	5.00	0.02	4.98	0.27
100	2017/01/18-15:16:10	42.6007	0.0300	13.3085	0.0260	6.85	3.86	-3.20e+22	1.20e+22	1.11e+22	5.57e+21	2.09e+22	6.97e+21	-1.55e+22	3.72e+21	1.50e+21	4.71e+21	-1.40e+22	3.52e+21	339	38	-63	127	56	-109	4.30	0.05	4.52	0.24
101	2017/01/18-19:32:31	42.5921	0.0200	13.2595	0.0110	11.86	2.82	-2.04e+22	7.81e+21	8.29e+21	5.88e+21	1.21e+22	3.23e+21	8.21e+21	2.48e+21	-1.30e+22	2.46e+21	-1.43e+22	3.35e+21	131	28	-101	324	62	-83	4.23	0.04	9.97	0.26
102	2017/01/19-10:25:50	42.6535	0.2700	13.2454	0.3040	7.61	14.34	-1.31e+21	4.85e+21	6.80e+20	4.99e+21	6.31e+20	7.36e+21	5.07e+20	5.63e+21	-1.17e+19	1.36e+21	-8.22e+20	2.90e+21	299	54	-108	148	39	-66	3.39	0.74	18.35	8.77
103	2017/01/21-03:54:24	42.6038	3.7940	13.3526	1.1720	3.13	35.80	-3.12e+20	1.34e+22	-5.08e+20	6.27e+22	8.20e+20	4.93e+22	-3.60e+20	1.26e+22	-3.86e+19	3.07e+22	-3.67e+20	1.04e+22	25	64	-23	125	68	-152	3.23	9.85	4.84	18.08
104	2017/01/21-09:35:55	42.7249	0.0120	13.2191	0.0130	1.63	4.02	-2.99e+21	1.58e+21	1.91e+21	9.69e+20	1.08e+21	2.05e+21	-5.78e+20	1.27e+21	1.94e+21	8.02e+20	-2.57e+21	7.01e+20	150	61	-66	287	36	-126	3.68	0.06	15.84	0.37
105	2017/01/27-14:20:15	42.5407	0.0170	13.3468	0.0260	9.90	2.08	-1.17e+21	5.14e+20	2.11e+20	1.17e+21	9.62e+20	9.53e+20	5.11e+20	7.14e+20	-1.21e+21	6.49e+20	-4.13e+20	5.95e+20	336	69	-89	155	20	-91	3.43	0.10	12.37	0.39
106	2017/01/28-16:14:40	42.6268	0.0480	13.3156	0.0430	2.91	2.78	-7.04e+20	1.05e+21	2.73e+20	6.29e+20	4.32e+20	1.36e+21	-3.92e+19	6.69e+20	-3.70e+20	6.14e+20	-5.93e+20	5.62e+20	340	57	-62	115	41	-126	3.25	0.21	11.59	0.43
107	2017/01/29-05:10:54	42.6330	0.0160	13.3029	0.0140	1.16	1.69	-6.17e+21	1.34e+21	2.54e+21	7.43e+20	3.63e+21	1.26e+21	4.84e+20	1.66e+21	-3.17e+20	1.52e+21	-3.89e+21	1.04e+21	317	47	-92	140	42	-87	3.82	0.04	12.40	0.38
108	2017/02/03-03:47:55	42.9915	0.0150	13.0219	0.0200	0.61	0.58	-6.29e+21	1.64e+21	-6.82e+19	2.02e+21	6.36e+21	1.59e+21	-1.65e+21	1.92e+21	3.08e+21	1.34e+21	-2.91e+21	1.09e+21	155	58	-94	343	31	-82	3.86	0.05	8.23	0.3
109	2017/02/03-04:10:05	42.9918	0.0160	13.0321	0.0160	0.43	1.02	-1.56e+22	4.41e+21	2.34e+21	3.04e+21	1.32e+22	2.83e+21	-3.14e+21	4.71e+21	4.46e+21	3.05e+21	-6.81e+21	1.80e+21	337	35	-84	151	54	-93	4.09	0.05	4.76	0.31
110	2017/02/03-05:40:34	43.0035	0.0050	13.0468	0.0140	1.58	1.48	-5.60e+21	1.41e+21	2.20e+18	9.39e+20	5.60e+21	1.22e+21	-5.54e+20	1.09e+21	2.12e+20	1.35e+21	-2.93e+21	1.09e+21	342	43	-81	151	47	-97	3.81	0.04	5.18	0.36
111	2017/02/03-23:37:43	42.6225	0.1920	13.3165	0.0230	7.77	6.61	-1.69e+21	4.40e+21	6.53e+20	2.05e+21	1.04e+21	2.94e+21	-4.68e+20	1.44e+21	9.37e+20	1.17e+21	-1.42e+21	1.77e+21	148	59	-78	306	32	-108	3.51	0.27	13.81	0.75
112	2017/02/04-02:39:13	42.9846	0.1020	13.0380	0.0540	-0.12	1.96	-8.09e+20	7.31e+20	-4.41e+19	8.72e+20	8.53e+20	2.92e+20	3.62e+20	1.28e+21	1.43e+20	2.02e+21	-4.02e+20	1.69e+21	315	50	-124	182	50	-55	3.27	0.27	41.28	7.1
113	2017/02/04-03:41:58	42.9895	0.0390	13.0484	0.0330	-0.58	2.93	-9.66e+20	9.71e+20	-8.50e+19	1.61e+21	1.05e+21	1.01e+21	-1.88e+20	5.72e+20	2.36e+20	1.40e+21	-9.62e+20	9.68e+20	143	51	-98	338	38	-78	3.37	0.17	11.05	0.34
114	2017/02/06-23:38:56	42.9804	0.1040	13.0370	0.0260	1.08	3.47	-2.20e+21	2.17e+21	3.00e+20	2.85e+21	1.90e+21	2.41e+21	5.56e+20	1.46e+21	1.07e+21	3.82e+21	-1.08e+21	4.69e+21	313	40	-123	174	57	-64	3.55	0.31	15.96	6.62
115	2017/02/09-09:58:27	42.6637	0.0050	12.6887	0.0060	1.62	0.70	-4.51e+21	5.03e+20	3.71e+21	4.24e+20	8.01e+20	4.12e+20	3.46e+20	4.65e+20	1.46e+20	3.17e+20	-3.03e+20	2.82e+20	273	47	-92	97	42	-87	3.68	0.02	7.79	0.36
116	2017/02/09-14:14:41	42.6806	0.0950	12.6858	0.0880	1.43	6.64	-9.97e+20	2.40e+20	7.80e+20	2.13e+21	2.17e+20	2.17e+21	2.80e+19	3.12e+21	1.35e+20	1.47e+21	1.21e+20	2.99e+21	252	47	-98	84	43	-81	3.25	0.33	5.10	7.43
117	2017/02/14-08:28:04	42.6913	0.0090	13.2210	0.0090	6.77	1.38	-2.19e+21	4.28e+20	3.58e+20	4.58e+20	1.83e+21	6.90e+20	1.67e+21	4.05e+20	-9.01e+20	3.94e+20	-1.28e+21	3.33e+20	310	65	-109	170	31	-54	3.59	0.04	1.61	0.38
118	2017/02/20-03:13:30	42.5038	0.0060	13.2676	0.0130	4.25	0.99	-8.38e+21	1.34e+21	2.05e+21	8.52e+20	6.33e+21	1.41e+21	-9.19e+20	1.50e+21	1.93e+21	1.54e+21	-3.37e+21	1.11e+21	330	37	-91	152	52	-88	3.89	0.03	6.01	0.38
119	2017/02/23-03:17:31	42.6019	0.0150	13.2346	0.0170	5.57	2.40	-1.64e+21	6.81e+20	3.50e+20	4.51e+20	1.29e+21	6.98e+20	4.26e+20	4.54e+20	-7.71e+20	4.81e+20	-6.30e+20	7.39e+20	332	59	-91	154	30	-88	3.45	0.08	9.72	0.38
120	2017/03/20-05:02:41	42.5714	0.0300	13.3748	0.0240	2.87	1.12	-3.72e+20	3.75e+20	-1.35e+21	5.43e+20	1.72e+21	5.03e+20	4.04e+20	3.27e+20	4.88e+20	4.36e+20	-6.91e+19	5.89e+20	314	65	-173	221	84	-24	3.42	0.06	25.58	0.42
121	2017/04/11-14:35:23	43.0176	0.0060	13.0967	0.0340	4.28	1.28	3.46e+20	3.74e+20	-1.91e+21	4.50e+20	1.56e+21	5.84e+20	2.71e+20	3.17e+20	4.62e+19	2.72e+20	-1.29e+21	7.73e+20	296	86	-174	206	84	-3	3.50	0.07	8.96	0.4
122	2017/04/11-14:45:26	43.0208	0.0870	13.1424	0.0590	1.34	11.91	3.45e+19	8.72e+20	-4.44e+20	4.26e+21	4.10e+20	3.41e+21	2.28e+20	4.07e+20	-9.74e+19	6.87e+20	-7.39e+20	7.74e+20	195	73	2	104	87	163	3.24	0.48	21.10	0.36
123	2017/04/11-17:04:56	43.0183	0.0090	13.1305	0.0290	1.97	3.13	-2.58e+19	2.89e+20	-1.01e+21	7.65e+20	1.04e+21	6.33e+20	5.54e+20	6.67e+20	-3.77e+20	5.05e+20	-1.77e+21	4.52e+20	195	73	4	104	85	163	3.49	0.06	20.37	0.43
124	2017/04/11-17:25:21	43.0326	0.1070	13.1318	0.0260	4.51	17.51	-2.21e+20	1.42e+21	-8.96e+20	3.27e+21	1.12e+21	2.40e+21	3.37e+19	4.13e+20	2.14e+20	1.06e+21	-5.08e+20	1.08e+21	31	88	9	301	80	178	3.31	0.44	9.35	7.8
125	2017/04/23-05:38:58	42.5649	0.0600	13.3710	0.0650	4.15	1.83	2.66e+20	8.04e+20	-1.24e+21	5.62e+20	9.75e+20	8.56e+20	5.48e+20	5.43e+20	1.89e+20	6.53e+20	-2.61e+20	8.93e+20	310	68	-174	218	85	-21	3.35	0.12	19.56	0.47
126	2017/04/27-21:16:58	42.9771	0.0110	13.0579	0.0090	0.85	0.33	-7.58e+21	6.63e+20	1.42e+20	1.18e+21	7.44e+21	1.10e+21	-2.25e+21	1.17e+21	2.87e+21	8.57e+20	-4.53e+20	8.24e+20	8	35	-68	162	57	-104	3.88	0.02	11.57	0.3
127	2017/04/27-21:19:42	42.9872	0.0270	13.0614	0.0130	0.66	1.13	-6.06e+21	1.48e+21	5.22e+20	7.65e+21	5.54e+21	7.64e+21	-1.40e+21	2.87e+21	3.81e+21	7.38e+21	-7.93e+20	9.05e+21	356	28	-79	165	62	-95	3.84	0.21	14.10	0.27
128	2017/05/19-04:46:53	42.7821	0.0140	13.2169	0.0190	7.11	1.96	-2.51e+20	1.50e+20	-1.14e+20	1.64e+20	3.65e+20	2.21e+20	8.18e+19	2.05e+20	8.59e+20	1.10e+20	-1.44e+20	2.79e+20	313	14	-140	185	80	-78	3.25	0.04	5.17	0.4
129	2017/05/26-07:57:03	42.7765	0.0470	13.2212	0.0490	3.49	2.89	-1.42e+20	1.59e+20	5.49e+19	4.96e+20	8.67e+19	5.15e+20	2.79e+20	1.79e+20	-2.60e+20	1.57e+20	-9.61e+18	3.37e+20	313	81	-92	150	8	-73	3.01	0.13	22.80	7.76
130	2017/06/02-00:21:46	42.8072	0.0070	13.2300	0.0160	7.42	1.84	-8.20e+20	2.29e+20	-1.60e+19	3.04e+20	8.36e+20	3.75e+20	1.21e+21	2.62e+20	1.03e+21	3.41e+20	-1.71e+20	3.85e+20	218	79	-73	339	20	-146	3.44	0.05	4.05	0.38
131	2017/06/24-08:30:04	42.8819	0.0420	13.1175	0.0280	3.87	2.27	-9.46e+20	5.61e+20	-2.11e+20	6.50e+20	1.16e+21	7.71e+20	1.87e+20	4.08e+20	-6.11e+20	5.90e+20	1.48e+20	7.44e+20	202	32	-64	352	61	-105	3.34	0.12	7.27	0.39
132	2017/06/29-21:41:21	42.6340	0.0090	13.2175	0.0080	8.35	1.90	-1.47e+21	3.71e+20	4.08e+20	4.55e+20	1.06e+21	6.95e+20	8.87e+20	4.54e+20	-1.68e+21	1.84e+20	-1.18e+21	5.98e+20	130	22	-109	331	69	-82	3.55	0.04	6.12	0.36
133	2017/06/30-00:25:17	42.6304	0.0100	13.2122	0.0120	6.05	1.18	-2.91e+21	1.30e+21	-6.00e+20	5.45e+20	3.51e+21	1.24e+21	3.27e+21	7.75e+20	-4.00e+21	9.15e+20	-1.25e+21	1.03e+21	188	21	-46	323	74	-104	3.80	0.04	7.72	0.41
134	2017/07/01-19:17:25	42.6509	0.0110	13.3088	0.0240	8.39	2.05	-1.56e+21	6.27e+20	2.44e+20	4.48e+20	1.32e+21	6.58e+20	-9.64e+20	8.18e+20	1.69e+21	7.72e+20	-1.18e+21	7.40e+20	149	68	-87	323	21	-96	3.56	0.07	5.61	0.34
135	2017/07/02-19:21:21	42.8676	0.0870	13.1751	0.1820	1.81	3.06	2.74e+20	1.93e+21	5.47e+19	1.56e+22	-3.29e+20	1.60e+22	-2.87e+20	3.62e+21	3.55e+20	2.07e+21	-2.32e+20	5.03e+21	346	72	54	234	39	151	3.12	2.59	61.48	9.17
136	2017/07/22-02:13:07	42.5713	0.0090	13.3852	0.0220	11.04	1.16	-8.21e+21	1.29e+21	2.88e+21	1.58e+21	5.33e+21	1.93e+21	8.79e+21	1.15e+21	-2.94e+21	1.97e+21	-1.02e+22	2.53e+21	171	36	-36	292	68	-120	4.06	0.04	5.03	0.26
137	2017/08/25-15:32:19	43.1267	0.0630	13.1937	0.0420	1.94	4.66	-3.86e+20	8.29e+20	-6.49e+20	1.33e+21	1.03e+21	9.43e+20	-6.27e+20	7.14e+20	4.11e+20	8.33e+20	-4.18e+20	1.83e+21	27	48	-16	128	78	-137	3.33	0.22	20.49	7.95
138	2017/09/01-10:29:31	43.0053	0.0300	13.0073	0.0410	7.89	6.71	-5.13e+19	3.05e+20	1.38e+20	3.51e+20	-8.72e+19	4.54e+20	1.04e+20	4.55e+20	1.14e+20	1.81e+20	-9.60e+20	5.07e+20	267	83	-173	176	83	-6	3.26	0.15	7.99	7.71
139	2017/09/04-18:54:02	42.5640	0.0370	13.3333	0.0490	7.59	2.15	-3.58e+20	6.22e+20	-4.65e+20	1.33e+21	8.23e+20	1.35e+21	5.20e+20	1.00e+21	-7.29e+20	9.04e+20	-2.20e+20	9.20e+20	211	31	-23	321	78	-119	3.31	0.23	7.68	0.47
140	2017/09/05-04:34:21	42.5813	0.0320	13.3525	0.0180	7.72	2.38	-2.55e+21	6.00e+20	-2.15e+21	8.34e+20	4.70e+21	1.08e+21	2.08e+21	1.07e+21	-2.83e+21	7.85e+20	-9.39e+20	6.13e+20	207	35	-32	324	71	-121	3.76	0.04	5.94	0.42
141	2017/10/19-05:34:54	42.8574	0.0490	13.2418	0.0700	2.72	12.75	3.73e+20	8.41e+20	2.24e+20	8.20e+20	-5.96e+20	1.58e+21	-2.22e+20	8.50e+20	6.07e+20	3.93e+20	1.80e+20	6.63e+20	186	20	116	338	71	80	3.22	0.24	25.93	7.94
142	2017/10/20-16:16:37	42.8118	0.0130	13.1503	0.0110	10.05	3.40	-2.97e+20	2.42e+20	4.07e+20	3.57e+20	-1.10e+20	4.86e+20	-5.11e+20	3.44e+20	6.27e+20	3.09e+20	-3.98e+19	5.32e+20	249	19	-153	134	81	-72	3.24	0.10	5.82	0.36
143	2017/11/02-18:04:14	42.6720	0.0590	13.1530	0.0470	11.86	7.48	1.12e+21	1.52e+21	-2.49e+21	2.02e+21	1.37e+21	2.33e+21	1.84e+20	3.16e+21	-1.68e+19	2.41e+21	-3.65e+20	2.05e+21	129	87	172	219	82	3	3.50	0.19	87.41	8.37
144	2017/12/03-23:34:11	42.6467	0.0120	13.3410	0.0180	2.28	1.15	-8.50e+21	2.55e+21	2.76e+21	2.32e+21	5.74e+21	1.81e+21	-6.57e+21	1.08e+21	4.61e+21	2.16e+21	-8.22e+21	2.61e+21	126	64	-105	338	29	-61	4.03	0.04	11.43	0.29
145	2018/01/11-03:48:02	42.6527	0.0320	13.3113	0.0320	5.35	3.13	-1.60e+21	8.58e+20	-1.04e+20	1.24e+21	1.70e+21	9.37e+20	2.71e+20	6.38e+20	1.59e+20	4.72e+20	-8.10e+20	6.79e+20	325	45	-109	172	47	-71	3.45	0.10	22.57	0.73
146	2018/02/04-12:45:33	42.6633	0.1750	13.3016	0.0540	8.40	6.24	-4.79e+20	1.37e+21	1.27e+20	2.89e+21	3.52e+20	1.89e+21	3.76e+20	1.10e+21	-3.36e+20	3.80e+21	-2.47e+20	2.80e+21	316	68	-98	158	23	-68	3.17	0.92	18.78	8.24
147	2018/03/08-22:48:46	43.0773	0.0100	13.0369	0.0300	6.38	2.30	-1.61e+21	1.16e+21	4.14e+20	6.67e+20	1.19e+21	9.08e+20	3.59e+20	6.18e+20	1.75e+20	4.37e+20	-1.33e+21	4.45e+20	305	49	-115	161	46	-63	3.47	0.09	7.79	0.44
148	2018/03/08-23:32:18	43.0790	0.0310	13.0302	0.0390	7.78	3.54	4.66e+19	1.91e+21	-2.21e+20	1.66e+21	1.74e+20	1.05e+21	3.84e+20	8.02e+20	1.85e+20	3.66e+20	-7.17e+20	6.05e+20	279	80	-157	184	67	-10	3.23	0.23	41.95	0.37
149	2018/03/26-22:43:07	43.0579	0.0670	12.9057	0.1200	1.38	6.63	-3.20e+20	1.31e+21	3.27e+20	1.75e+21	-6.90e+18	9.08e+20	-3.48e+20	7.42e+20	-2.76e+20	6.04e+20	-3.96e+20	7.96e+20	336	49	-30	87	67	-135	3.16	0.36	16.84	3.41
150	2018/04/04-02:19:45	43.0936	0.0290	13.0390	0.0300	4.10	2.78	-7.55e+21	4.68e+21	-7.76e+20	3.95e+21	8.33e+21	3.20e+21	1.00e+21	2.23e+21	2.87e+21	1.88e+21	-7.00e+21	1.61e+21	305	45	-129	175	56	-56	3.97	0.06	19.78	0.24
151	2018/04/04-18:41:28	43.0769	0.0630	13.0308	0.0550	6.95	4.94	-3.68e+21	4.86e+21	-3.63e+20	7.93e+21	4.04e+21	3.34e+21	4.29e+20	7.62e+20	5.12e+20	1.95e+21	-1.85e+21	8.68e+20	328	43	-107	171	48	-74	3.70	0.18	11.30	0.37
152	2018/04/10-03:11:30	43.0818	0.0120	13.0254	0.0150	6.29	1.37	-6.10e+22	6.59e+21	3.18e+22	1.12e+22	2.92e+22	1.36e+22	-1.32e+22	6.61e+21	3.80e+22	6.90e+21	-4.06e+22	5.11e+21	148	61	-73	297	32	-116	4.53	0.02	8.03	0.23
153	2018/04/11-00:00:51	43.0683	0.0240	13.0334	0.0230	4.13	7.86	-4.58e+20	2.65e+21	-3.30e+20	1.37e+21	7.88e+20	1.51e+21	-4.57e+19	7.83e+20	2.43e+20	8.76e+20	-6.87e+20	1.18e+21	197	83	-19	289	70	-172	3.27	0.35	32.28	0.74
154	2018/04/12-13:24:03	43.0722	0.0100	13.0566	0.0530	7.14	4.73	-2.96e+20	1.11e+21	6.79e+20	7.26e+20	-3.84e+20	8.90e+20	2.90e+20	6.61e+20	7.60e+20	3.63e+20	-1.36e+21	4.86e+20	263	65	-163	165	74	-25	3.42	0.08	9.99	0.34
155	2018/04/25-01:08:16	43.0720	0.0200	13.0368	0.0420	7.92	2.26	-1.24e+21	3.48e+20	7.49e+20	5.15e+20	4.94e+20	4.87e+20	6.62e+20	3.10e+20	1.03e+21	2.84e+20	-1.20e+21	3.21e+20	281	51	-139	163	59	-45	3.47	0.04	18.44	0.67
156	2018/05/21-08:49:26	43.0955	0.0080	13.0208	0.0120	8.84	2.67	-8.27e+21	1.61e+21	7.88e+20	8.21e+20	7.48e+21	1.53e+21	2.01e+19	1.18e+21	4.45e+21	8.90e+20	-4.30e+21	8.59e+20	320	34	-112	166	58	-75	3.94	0.03	7.28	0.39
157	2018/05/21-12:38:35	42.6198	0.0120	13.3202	0.0140	7.22	2.25	-7.65e+20	2.30e+20	-5.03e+20	2.18e+20	1.27e+21	2.39e+20	5.82e+20	1.98e+20	-1.96e+20	1.41e+20	2.45e+20	2.03e+20	335	59	-137	220	53	-38	3.34	0.04	11.51	0.38
158	2018/07/21-08:01:50	43.0860	0.0270	13.0213	0.0200	9.63	9.94	-5.27e+20	3.33e+21	-1.12e+20	1.37e+21	6.39e+20	3.85e+21	2.65e+20	6.79e+20	1.36e+20	8.76e+20	-4.48e+20	1.41e+21	304	54	-135	185	55	-45	3.21	0.75	27.29	6.61
159	2018/09/11-21:57:13	42.9451	0.0100	13.2005	0.0100	1.44	1.36	-1.25e+21	2.68e+20	1.35e+20	1.61e+20	1.11e+21	2.62e+20	-1.42e+20	3.20e+20	-4.14e+19	3.49e+20	-1.58e+20	1.59e+20	357	45	-81	165	44	-98	3.32	0.05	8.42	0.39

Centroid Moment Tensor catalog with 3D lithospheric wavespeed model: the 2016–2017 Central Apennines sequence

P. Artale Harris[1], L. Scognamiglio[1], F. Magnoni[1], E. Casarotti[1]and E. Tinti[1,2]

[1]Istituto Nazionale di Geofisica e Vulcanologia, Roma
[2]Sapienza Universitá di Roma

Key Points:

- A new centroid moment tensor catalog for Central Italy earthquakes has been build based on a 3D wavespeed model for the Italian lithosphere
- Moment magnitude and kinematic source parameters are well constrained; centroid depths with the 3D wavespeed model are accurately estimated
- The goodness of moment tensor solutions is tested via a newly designed quality factor

Corresponding author: Pietro Artale Harris, `pietro.artale@ingv.it`

Abstract

Moment tensor inversions of broadband velocity data are usually managed by adopting Green's functions for 1D layered seismic wavespeed models. This assumption can impact on source parameter estimates in regions with complex 3D heterogeneous structures and rock properties discontinuities. In this work, we present a new Centroid Moment Tensor (CMT) Catalog for the Amatrice–Visso–Norcia (AVN) seismic sequence based on a recently generated 3D wavespeed model for the Italian lithosphere. Forward synthetic seismograms and Fréchet derivatives for CMT–3D inversions of 159 earthquakes with $M_w \geq 3.0$ are simulated using a spectral–element method (SEM) code. By comparing the retrieved solutions with those from Time Domain Moment Tensor (TDMT) catalog, obtained with a 1D wavespeed model calibrated for Central Apennines (Italy), we observe a remarkable degree of consistency in terms of source geometry, kinematics, and magnitude. Significant differences are found in centroid depths, which are more accurately estimated using the 3D model. Finally, we present a newly designed parameter, τ, to better quantify and compare a–posteriori the reliability of the obtained MT solutions. This parameter measures the goodness of fit between observed and synthetic seismograms accounting for differences in amplitude and arrival time, percentage of fitted seconds, together with the usual L2–norm estimate. These CMT–3D solutions represent the first Italian CMT catalog based on a full–waveform 3D wavespeed model and provide robust source parameters with potential implications for the structures activated during the sequence. The developed approach can be readily applied to more complex Italian regions where a 1D wavespeed model is underperforming.

Plain language summary

The moment tensor (MT) is a mathematical representation of the movement on a fault during an earthquake and of the size, or magnitude, of the event. Such tensor is often described through the beachballs, a graphic symbol that indicates the fault orientation and the type of slip that occurs during an earthquake. Usually, seismologist use 1D wavespeed models (*i.e.* describing only the vertical velocity of seismic waves in the earth interior) in order to compute MTs. In recent years, due to the incredible progresses of the computer sciences, also 3D models, which are able to describe lateral velocity variations, have been successfully adopted to compute MTs. In this work, we use the recently developed 3D Italian wavespeed model 'IMAGINE_IT' to compute the MTs solutions for the Amatrice-Visso-Norcia 2016—2018 earthquakes with magnitude larger than 3. This seismic sequence ruptured almost 80 km of the Apennines normal faults and resulted in 299 casualties and more than 20,000 homeless. Our newly developed MTs catalogue allowed us to better understand the characteristics of the faults activated during the seismic sequence and to provide more robust source parameters as magnitude and depth.

1 Introduction

The Amatrice–Visso–Norcia (AVN) seismic sequence began on August 24th, 2016, with the M_w 6.0 earthquake close to the town of Amatrice, and was marked by three main events in two months culminating in the M_w 6.5, October 30th, 2016, Norcia event (Figure 1). Between August 2016 and September 2018, the sequence ruptured almost 80 km of the Apennines high–angle normal faults, dipping 46°–60°, and activated a nearly horizontal detachment at $\sim 8 - 12$ km depth (Chiaraluce et al., 2017; Scognamiglio, Tinti, & Quintiliani, 2016; Michele et al., 2020). The mainshocks broke two of the most important extensional fault systems of this portion of the Apennines mountain belt owning to two different geologic domains: the Mt. Vettore–Mt. Bove fault system (VBFS) to the North, in the Umbria–Marche domain, and the Mt. della Laga fault system (LMFS) to the South, in the Latium–Abruzzi domain. These fault systems are separated by a major regional tectonic structure, the NNE–SSW–trending lateral ramp of the Olevano Antodoco Sibillini (OAS) thrust, inherited from the Miocene–Pliocene compressional tectonic phase (Barchi et

al., 1998a, 1998b; Lavecchia, 1985). Location, depth, and prevalent normal faulting mechanisms indicate that the sequence originated in the shallow crust of the Apennines chain where the current extensional regime overprints contractional structures. Structural complexity plays a major role in fault segmentation and interaction in this region, with important consequences on seismic behavior and mechanics of earthquake faulting. This complexity is evidenced by the co–existence of fault planes with different focal mechanisms in the same area (Chiaraluce et al., 2017; Scognamiglio, Tinti, & Quintiliani, 2016; Scognamiglio et al., 2018; Michele et al., 2020).

A current Moment Tensor (MT) Catalog for the AVN seismic sequence contains well–constrained solutions down to $M_w = 3.0$ and it is published in the INGV website (`http://terremoti.ingv.it/tdmt`). The Time Domain Moment Tensor (TDMT) solutions (Scognamiglio et al., 2009) downloadable from this website are obtained using a 1D wavespeed model, called *CIA* (Herrmann et al., 2011), which has been built ad–hoc for the Central Italy region. Such a wavespeed model allows for robust solutions and good fits for the whole AVN sequence. However, the quality of fit for stations with distances larger than ~ 300 km from the source tends to deteriorate due to the heterogeneities characterizing the Italian lithosphere even at low frequencies ($\sim 0.02 - 0.1$ Hz).

It is well–known that a high–quality focal mechanism catalog is of crucial importance to obtain good constraints on regional stress field, assess to earthquake hazards, and understand tectonic processes. The usual procedure to determine moment tensors (or focal mechanisms) for small to moderate earthquakes considers simple local or regional 1D Earth wavespeed models (Scognamiglio et al., 2009; Herrmann et al., 2011; Yang et al., 2012). However, some regions are characterized by strong 3D heterogeneities, which can range from local to regional scales (Wang & Zhan, 2019; Takemura et al., 2021), and the adoption of 1D models in inverting observed waveforms may cause errors and therefore contribute to uncertainties on moment tensor solutions (Wang & Zhan, 2020; Hingee et al., 2011; Scognamiglio, Magnoni, et al., 2016). In many cases the effects of the 3D Earth structure have to be included, especially to take into account the uneven distribution of the stations used to perform the inversion. Moreover, the effects of the lateral Earth variations may be of crucial importance when considering small–to–moderate–sized earthquakes with only high signal-to-noise ratio (S2NR) waveforms at short periods (Zhu & Zhou, 2016; Wang & Zhan, 2019).

Seismic tomography and full–waveform inversion have made incredible progresses. Thanks to recent improvements in computational resources as well as forward solvers (e.g., Peter et al., 2011), the generation of very accurate 3D models become feasible. The inclusion of a good 3D wavespeed model, when available at the appropriate resolution scale, could be now considered as a reasonable procedure when publishing seismic source solutions. Moreover, a more accurate evaluation of source parameters can be used for hazard assessment, with possible crucial lapels for all the citizens.

In recent years, numerous studies that illustrate the advantages of 3D wavespeed models to build MT catalogs have been published. These advantages span from the field of microseismicity (Collins et al., 2014; Li et al., 2021) to induced seismicity (Chiang et al., 2019; Willacy et al., 2019), from continental (Covellone & Savage, 2012; Hejrani et al., 2017) to local seismology (Scognamiglio, Magnoni, et al., 2016; Hingee et al., 2011; Takemura et al., 2020; Wang & Zhan, 2019). Moreover, the use of 3D models goes together with the use of new MT inversion methodologies (Fichtner & Simuté, 2018) that include probabilistic seismic point source inversion analyses (*i.e.*, Hamiltonian Monte Carlo Inversion).

One of the most important results when using 3D wavespeed models is to obtain better constraints of the kinematic parameters (Hingee et al., 2011) and better waveform fit (Covellone & Savage, 2012; Nayak & Dreger, 2018). The computation of high quality moment tensor solutions can also affect the assessment of the earthquake size and depth. Takemura et al. (2021) show that 1D wavespeed model systematically overestimate the M_w when compared with their local 3D model, while Hjörleifsdóttir and Ekström (2010) and

Wang and Zhan (2019) point out that better depth constraints are obtained when considering 3D instead of 1D wavespeed model. Moreover, Wang and Zhan (2020) conclude that using 3D wavespeed models for MT computation allows to resolve the subsurface fault geometries which are fundamental to understand the kinematic of the activated structures. The possibility of constraining off–shore solutions is also of great importance. Takemura et al. (2018, 2020), computing Centroid Moment Tensor (CMT) inversions of earthquakes along the Nankai Trough (Japan), demonstrate that using a 3D wavespeed model improves the source parameters estimate for off–shore earthquakes, especially in terms of dip angles and centroid depths. Finally, the increase of double–couple percentage of the solutions in regions with complex heterogeneous structures is common when using 3D wavespeed models (Covellone & Savage, 2012; Hejrani et al., 2017; Wang & Zhan, 2019; Jechumtálová & Bulant, 2013).

In order to assess the described advantages in using a 3D model, in this study we report on reviewed source geometries of the AVN sequence as retrieved by moment tensor analysis performed for small to moderate–sized earthquakes based on a new 3D wavespeed model of the Italian lithosphere (Magnoni et al., 2021). Our goal is to investigate whether the adoption of a 3D elastic structure improves resolution in estimated source parameters, fault geometry and faulting styles. Finally, we define a *quality parameter*, in order to quantify the goodness of the obtained solutions. Such parameter evaluates the quality of the data fit and is calculated by considering the differences between recorded and synthetic data in cross–correlation, amplitude, timing and length of fitted seconds (Section 2.3). Therefore our ability to calculate a model that reproduces the kinematics of earthquakes is no longer defined only by a Variance Reduction (VR, as usually done when assessing the quality of fit) but takes into account other characteristics of the signal.

2 3D Centroid Moment Tensor Inversion

In this Section we present the data set and procedures used to compute the 3D Centroid Moment Tensor (CMT–3D) solutions, and how we evaluate the solution quality.

2.1 Data Set

We examine 159 earthquakes with $M_w \geq 3.0$ belonging to the studied area (longitude 12.7°–13.6°; latitude 42.45°–43.1°) and occurred between August 2016 and September 2018. The events' hypocentral location (`http://terremoti.ingv.it`) is computed by analysts of the seismic monitoring center at Istituto Nazionale di Geofisica e Vulcanologia (INGV). We use three–component broadband velocity waveforms recorded by the Italian National Seismic Network (IV), the MedNet Seismic Netowk (MN), the North–East Italy Seismic Network (OX), the CEA/DASE Seismic Network (RD), the Seismic Network of the Republic of Slovenia (SL), the INGV Experiments Network (TV), and the AlpArray Seismic Network temporary components (Z3). Raw data are downloaded through the INGV web services, checked for signal–to–noise ratio (S2NR) larger than 3, corrected for the instrument response, resampled at 1 sample per second and filtered by applying a low–pass and a high–pass causal (one pass and three poles) filter. The filter frequency range is magnitude–dependent: 0.02–0.05 Hz for earthquakes with $M_L \geq 3.95$ and 0.02–0.1 Hz for $M_L < 3.95$. The same filtering and resampling process is applied to synthetic traces (Section 2.2). The horizontal components are rotated to great circle path.

2.2 Inversion

We follow the point–source MT inversion procedure proposed by Liu et al. (2004) (`https://github.com/UTCompSeismo/GRD_CMT3D`) by using the python code "pycmt3d" (`https://doi.org/10.5281/zenodo.56124`). This technique permits to invert for CMT by numerically calculating the Freéchet derivatives of a waveform misfit function with re-

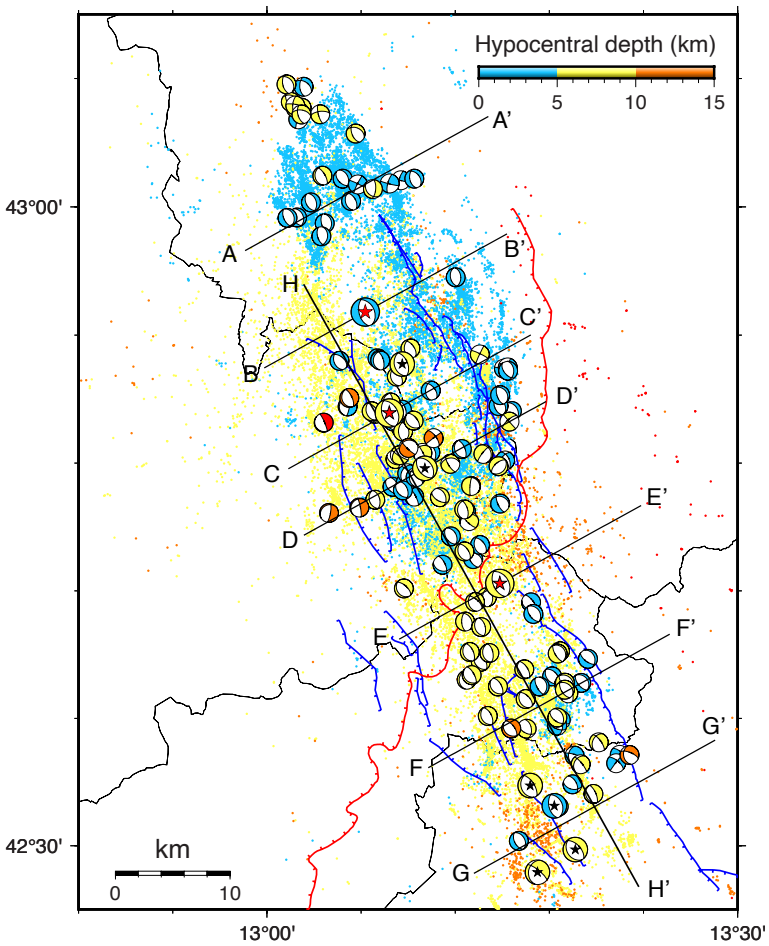

Figure 1. Map view of the study area. Dots represent earthquakes from Michele et al. (2020) while beachballs are focal mechanism solutions for the 136 events (among 159) with at least a 'fair' quality (see Section 3) obtained in this study; both are color–coded by depth. Enlarged beachballs with red stars are events with $M_w \geq 6.0$; beachballs with black stars are events with $5 \leq M_w < 6.0$. Black lines represent cross–section profiles. Red line represents the Olevano–Antrodoco–Sibillini (OAS) thrust front trace (modified after Centamore & Rossi, 2009) while blu lines represent mapped normal faults (Pucci et al., 2017, and references therein).

spect to the considered source parameters and then minimizing this misfit between data and synthetics (Liu et al., 2004).

Considering the TDMT solutions as starting solutions, the synthetic seismograms for the considered events are computed together with synthetic seismograms for perturbed source parameters, *i.e.*, the Freéchet derivatives for the six MT components and the three source location parameters. To simulate full synthetic waveforms we use the spectral-element method (SEM) code SPECFEM3D_Cartesian (Peter et al., 2011), which allows for accurate simulations in complex heterogeneous media.

Since our goal is to produce an MT catalog based on a reliable Earth structure, the wavespeed model used in the simulation code is the 3D model *Im25* (Magnoni et al., 2021), which has been recently obtained for the Italian lithosphere by an adjoint 3D full–waveform

travel–time tomography. *Im25* is a regional model for V_p and V_s at unprecedented resolution (down to a period of ∼10 s; Figure S1). For this model, the quality factor Q is obtained as a linear function of V_s, and the values of density ρ are calculated as a quadratic function of V_p based on an empirical relationship (Magnoni et al., 2021).

Before the MT inversion, we use the FLEXWIN windowing code (Maggi et al., 2009) in order to select the time windows, on recorded and synthetic seismograms, suitable for making phase and amplitude measurements and performing the inversion. Only earthquakes with at least 10 time windows are inverted (Magnoni et al., 2021). The time window selection is done via user–tunable parameters by imposing threshold values for cross–correlation, amplitude ratio and time–shift (see definitions in Maggi et al., 2009) between synthetics and observables. We choose the following requirements of goodness of fit to be satisfied by these quantities: cross–correlation ≥ 0.8, $|\text{amplitude ratio}| \leq 0.8$, $|\text{time–shift}| \leq 5$s or $|\text{time–shift}| \leq 7$s for $M_L < 3.95$ or $M_L \geq 3.95$, respectively. In addition to the above parameters, we modified the original FLEXWIN code by adding a new selecting condition: $vr \geq 0$, where vr is the window–variance reduction defined as:

$$vr = \left(1 - \frac{\int_{win}(x_{win} - d_{win})^2 \mathrm{dt}}{\int_{win} d_{win}^2 \mathrm{dt}}\right) \times 100\%; \tag{1}$$

here d_{win} and x_{win} are the data and synthetic time series within the window.

In FLEXWIN we also check the S2NR within each time window, by imposing its minimum threshold to be equal to 4.0. With this strong constraint, 30 earthquakes among 159 are excluded from the analysis. For theses events we lower the S2NR threshold for the time windows to 3.0 and carefully verify the goodness of the selected windows.

The code pycmt3d performs the moment tensor inversion considering only the selected windows for each pair of real and synthetic seismograms. A zero–trace constraint is always imposed during the CMT inversion, thus implying the isotropic MT component to be zero. The synthetics for the new CMT solutions are constructed by pycmt3d as a combination of the calculated Fréchet derivatives.

During the MT inversion, the code perturbs the initial solution to explore the space parameters. The perturbation for each moment tensor component is chosen as the maximum order of magnitude of the MT components of the given earthquake. For most of the events, latitude and longitude perturbation is 0.18°, and depth perturbation is 8 km. For three shallow events, we reduce the depth perturbation to 3 km to avoid non–physical solutions, that locate earthquakes above the local topography. For the mainshocks' hypocenters, which are already widely studied, we reduce the latitude, longitude and depth perturbation to 0.045° and 5 km, respectively.

The average computation time to produce a CMT–3D solution is ∼24 hours for the largest events ($M_L \geq 3.95$) and ∼13 hours for the smallest ones ($M_L < 3.95$) using 150 CPU cores on the INGV local cluster. The most computationally expansive operation is the time windowing through FLEXWIN, which can take up to 12 hours due to the increasing number of stations (and thus windows) for increasing magnitude events. The simulations of synthetics and Fréchet derivatives take ∼12 hours, while the inversion part as well as the processing take no more than 10 minutes.

2.3 Evaluation of the solutions

To provide an a–posteriori quantitative estimate of the MT solution quality we define a parameter τ inspired by the metric proposed by Covellone and Savage (2012). τ quantifies the capability of the source solution of modelling the real data and therefore of giving a reasonable estimate of the seismic source parameters. For each analysed event we compute

τ as:

$$\tau = C_\tau \frac{\sum w_m \bar{m}}{\sum w_m}. \tag{2}$$

C_τ is a sigmoid–like function such that its value is $\sim$1 for a number of windows greater or equal to 10, while the value increases for a smaller number of windows:

$$C_\tau = 1 + \frac{1}{e^{b(x-a)}}, a = 8, b = 2; \tag{3}$$

here x is the number of windows. With this choice, $C_\tau = 2$ if the number of windows is 8. The parameter $\bar{m}$ in Eq. 2 is defined as:

$$\bar{m} = \{\overline{dA}, \overline{\text{Tshift}}, \overline{\text{1-CC}}, \overline{\text{1-vr}}, \mathit{fits}\}, \tag{4}$$

where the bar symbol stands for the average of the considered parameters. Here 1-vr is based on the definition in Eq. 1, Tshift and CC are the FLEXWIN time–shift and cross–correlation parameters, respectively. To define the parameter dA we applied some algebra starting from the definition of the amplitude–ratio $dlnA$ in FLEXWIN (Maggi et al., 2009):

$$dlnA = \frac{1}{2} \ln \frac{\int_{win} d^2_{win} \mathrm{dt}}{\int_{win} x^2_{win} \mathrm{dt}}, \tag{5}$$

thus

$$1 - \exp 2dlnA = \frac{\int_{win} (x^2_{win} - d^2_{win}) \mathrm{dt}}{\int_{win} x^2_{win} \mathrm{dt}} =: dA. \tag{6}$$

From Eq. 6, we note that $1 - dA$ is directly proportional to the difference of the seismic wave energy. Finally, the parameter $\mathit{fits} = 1 - N_{\text{fitted}}/N_{\text{tot}}$, where N_{fitted} is the length of the inverted window and N_{tot} the total analysed seconds for each event.

w_m in Eq. 2 are the weights of the corresponding parameters in Eq. 4, *i.e.*, we use the standard deviation of the parameters except for the case of *fits* for which we have $w_{fits} = 0.1$.

The averages of the parameters in Eq. 4 are computed considering their values in each window of the given event, and are weighted by the duration of the windows. In the cases of dA and Tshift, we also normalize the averages by their maximum possible values. For Tshift we choose $T_{\max} = 7$, while for dA we have that the condition $|dlnA| \leq 0.8$ (Subsection 2.2) implies

$$-3.95 < dA < 0.8,$$

thus we choose $dA_{max} = 4$. An example of a fit, including the window parameters used to evaluate τ, can be found in Figure S2.

Based on the well–defined physical meaning of each parameter in τ (Eq. 2), we consider an "excellent" fit for values of τ from 0 to 0.25, a "good" fit from 0.25 to 0.50, a "fair" fit from 0.50 to 0.75, and for values above 0.75 an "unresolved" fit.

3 Results

We calculated a total of 159 CMT–3D solutions for small to moderate earthquakes occurred during the AVN seismic sequence. Estimated moment magnitudes M_w range from 3.01 to 6.43 and depths from -0.6 km to 15.1 km (see Table S1 and the ".csv" Table in the supplementary material for source parameters values and associated uncertainties). Most of the retrieved solutions show NW–SE normal fault mechanism confirming the well–known northeast–trending tectonic extension of this portion of the Apennines (Boncio et al., 2004; Chiarabba et al., 2005; D'Agostino et al., 2009; Carminati & Doglioni, 2012, for a review). Nevertheless, strike–slip, transtensional and low angle normal fault mechanisms exist, suggesting that structural complexities influence the pattern of seismicity (Figure 1).

Following the newly developed metric τ for MT solution quality estimation, we found that 83.1% of the retrieved solutions show a good or excellent fit between data and synthetics ($\tau \leq 0.50$, green beachballs in Figure 2), while 14.5% have $\tau \geq 1.00$ and a poor fit caused by the small number of the selected time windows (less than 8, displayed as unresolved solutions, red beachballs). The MT unresolved solutions belong to the smallest magnitude earthquakes of the catalog or to events occurred immediately after the Amatrice and Norcia mainshocks. Indeed, the time proximity of a mainshock causes the overlap and interference of phases from the two events. The remaining 2.4% solutions show a satisfactory fit (yellow beachballs).

3.1 Comparison with the TDMT catalog

To evaluate the quality of our CMT–3D solutions, we compare source mechanisms and moment magnitudes to those from the TDMT catalog, one of the reference catalogs for the Italian seismicty.

Mechanisms are compared through the Kagan rotation angle, which is defined as the minimum rotation about any axis that is needed to transfer from one focal mechanism to the other (Kagan, 1991). This angle ranges between $0° - 120°$ and allows us to quantitatively describe the dissimilarity between two focal mechanism solutions. We found an excellent consistency between the two catalogs (Figure 3a): less than 7% of the focal mechanisms have a rotation angle larger than 30°, which is generally considered the threshold for a good quality solution (Bernardi et al., 2004). Similarly to the large τ values, most of the larger Kagan values are mainly related to solutions with a small number of inverted windows and/or small magnitude events. Several of the kinematically diverging solutions come out with a high τ value, confirming the suitability of the developed quality parameter for moment tensor quality estimation.

Figure 3b shows the comparison between the two catalogs' M_w estimates for the 136 events with $\tau \leq 1.00$. Differences between M_w are very small, almost all the values are within the interval ± 0.1, giving us a good constraint on the retrieved solutions and on the accuracy of the estimated value. This is a noteworthy result, since M_w is the reference estimate of earthquake size both for scientific and non–scientific community. We can also observe that the CMT–3D M_w values are plotted together with their uncertainties (see Text S1 and the ".csv" Table in supplementary material): this is an important feature which contributes to assess the robustness of the result. As better illustrated in the Figure 3b inset, only 7 events among the 146 plotted have uncertainties larger than 0.2 (green dots).

For scientists, a realistic and well–constrained M_w value is needed for computing ground–shaking scenarios or when dealing with ground motion assessment, because it directly impacts the amplitude of the simulated ground motion. Instead, common people perceive the magnitude as an absolute and perpetual value so discrepancies on this parameter estimate could lead to misunderstanding and debates (La Longa et al., 2014; Scognamiglio, Tinti, & Quintiliani, 2016).

We also compare our centroid depths to those derived from TDMT, whose solutions are inferred exploring a range of depths discretized every 1 km around the initial depth (Figure 3c). We observe a large discrepancy between the two catalogs, probably due to limited depth resolution of the TDMT procedure, together with the use of a simplified 1D model, although well calibrated for the area. Our results suggest that incorporating the 3D wavespeed model in source inversions can improve the focal depth assessment. For sake of readability, we decided to avoid plotting uncertainties on CMT–3D depth values, those are all reported in the ".csv" Table in the supplementary material.

Finally, with an additional analysis, we studied if the retrieved M_w values satisfy the scaling relationship between M_L and M_w recently proposed for Central and Northern Apennines by Malagnini and Munafó (2018). By comparing for the 49 coinciding events, our M_w

Figure 2. Catalog of the retrieved solutions for the 159 CMT—3D events. The beachballs on the left are colored according to τ definition while the black beachballs on the right are the TDMT input solutions. M_w values are those of the CMT–3D solutions.

estimates with their M_L, computed by using a regionally calibrated attenuation relation (Munafò et al., 2016), we fit within one standard deviation the bilinear regression with the crossover at M_L=4.3 proposed by these authors (Figure 3d, and text S1 in Supplementary Material). This result further corroborates the reliability of the obtained M_w estimates which consequently behave as the M_w values of Malagnini and Munafó (2018).

3.2 Earthquake hypocentral location: constraining the tectonic structures

To further constrain the subsurface fault geometries and faulting styles of the tectonic structures that were activated during the AVN sequence, we compare our new CMT–3D catalog with the double difference relative locations of Michele et al. (2020), the best available at the time of writing. Locations and focal mechanisms from moment tensor solutions are overlapped in map–view, color–coded by depth (Figure 1), but also shown in a longitudinal cross–section, oriented N151°, and seven vertical cross–sections, oriented orthogonal to the longitudinal one (Figure 1,4–6). Vertical cross–sections include events within 2 km (*i.e.* ±2 km) from the profiles.

For common events, we find a general good agreement between the epicentral locations. Histograms of longitude and latitude distances have an almost normal distribution with mean $\mu = [-0.005°, -0.002°]$ (see Figure S3) for longitude and latitude, respectively, and an identical standard deviation $\sigma = 0.017°$, suggesting a slightly displaced location toward north–east for CMT–3D solutions. This is likely related to the different wavespeed models adopted to built the two catalogs. The map (Figure 1) shows that most focal mechanisms match in color with the background seismicity and coherently characterize the extensional kinematic of the main fault plains and their antithetic structures (Tinti et al., 2016; Scognamiglio, Tinti, & Quintiliani, 2016; Scognamiglio et al., 2018; Cheloni et al., 2019; Walters et al., 2018).

Moving from NW to SE along the AVN sequence strike direction, we discover the relationship between aftershocks and focal mechanisms. Aftershocks in cross-section A–A' delineate a synthetic–antithetic fault system (Figure 4a). Focal mechanism locations and dips agree with the event distribution and highlight that this system hosted some of the larger magnitude earthquakes occurred in this area (up to M_w=4.1). The shallower northwestern events nucleated on the antithetic fault, while the deeper ones, between 3 and 6 km, are located close to the synthetic fault. The deepest normal mechanism is the M_w 4.09 event, the first $M_w \geq 4.0$ event occurred in this area. It happened few hours after the Visso mainshock and is located close to the low–angle fault shear zone (SZ) which has been previously identified by Chiaraluce et al. (2017), Michele et al. (2020) and Lavecchia et al. (2017). This seems to support the hypothesis that 'seismic activity on the SZ responded passively to triggering by the shallow normal–faulting earthquakes' (Tan et al., 2021). The lowest dip angle of the considered mechanism is 33° and is related to the SW–dipping plane, that is in the opposite direction with respect to the dip delineated for the SZ by the studies on aftershocks (Chiaraluce et al., 2017; Improta et al., 2019; Michele et al., 2020). This feature has been already observed by Michele et al. (2020) and agrees with the idea that the events nucleating close to the SZ may dislocate higher angle planes as a brittle response to the sub-horizontal deformation process. The A–A' section also contains three strike–slip focal mechanisms. The role of the strike–slip kinematic cannot be easily inferred from the aftershocks' distribution, since no vertical event alignment is found even if we change the cross–sections' azimuth according to their strike values. These earthquakes are probably associated to minor structures that accommodate the overall tectonic deformation.

Moving toward southeast, we explore the correlation between MT solutions and the faults where Visso and Norcia earthquakes nucleated. Seismicity in the section crossing the Visso mainshock (Figure 4b) slightly describe a southwest–dipping plane. The portion of the fault around the Visso hypocenter, located at 4.6 km depth, appears almost as a shadow area for the aftershock distribution. This feature could be explained with the commonly observed

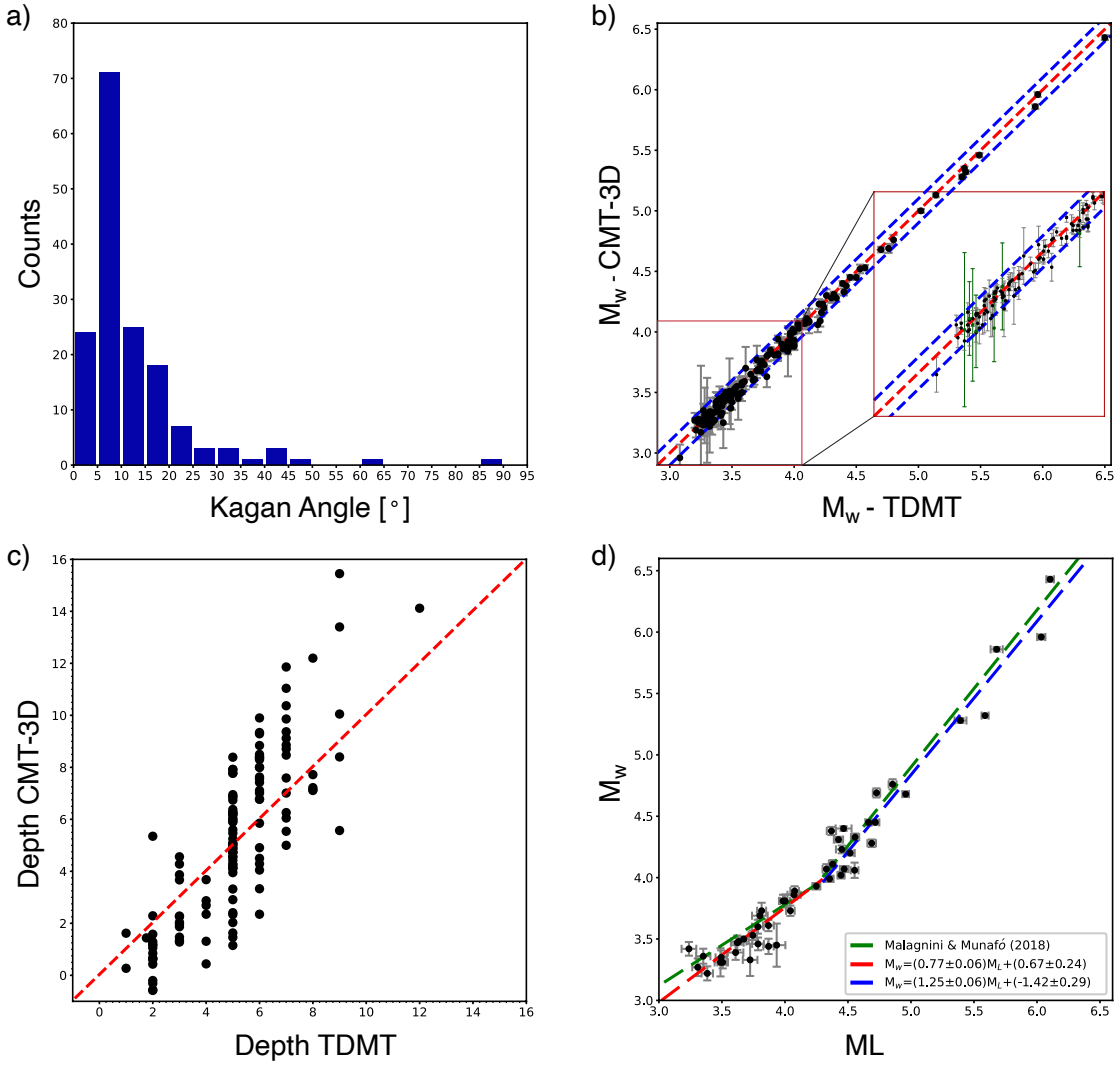

Figure 3. Comparison between CMT–3D solutions (this study) and TDMT earthquake catalog and $M_L - M_w$ regression. a) Histogram of the focal mechanism rotation angle (Kagan angle) between the catalogs; b) Plot of the earthquakes' M_w. Red and blue lines show the 1:1 linear fit and the ±0.1 interval, respectively. The uncertainties on the CMT–3D M_w values are superimposed for identical values of M_w from TDMT. The red box in the inset is a zoom of the 2.9-4.1 magnitude range where the green dots highlight the 7 events with uncertainties value larger than 0.2; c) comparison of centroid depth between TDMT and CMT–3D inversion methodology; d) $M_L - M_w$ regression.

anticorrelation between aftershocks and main slip release fault area. Indeed, the finite–fault model proposed by Chiaraluce et al. (2017) shows that the slip is entirely distributed on an elongated patch of 8×4 km at depths between 3.5 and 6.5 km that well agree with the lack of aftershocks. This portion of the fault system hosts two CMT–3D solutions, the mainshock, whose centroid location and focal mechanism are perfectly consistent with the fault plane, and a shallower mechanism which could suggest a dip–slip southwest–dipping kinematic for the eastern events aligned in parallel to the mainshock's fault.

In section C–C', which hosts the M_w 6.5 Norcia earthquake, the aftershock distribution images a quite complex geometry of activated faults whose kinematic is explained by the retrieved CMT–3D solutions (Figure 4c). These solutions clearly describe the mainshock's fault plane dipping 47°SW. Two other CMT–3D solutions lie along the shallow part of this highlighted plane and confirm the geometry and the kinematic of this structure. It is interesting to note that the two solutions belonging to the main fault plane are related to the seismicity active before the Norcia earthquake. Both in the hangingwall and in the footwall of the mainshock's fault, a clustered seismicity suggests the existence of two NE–dipping antithetic faults and the CMT–3D solutions located close to these faults are consistent with this hypothesis. Once again, the eastern strike–slip retrieved solutions cannot be associated with vertical aftershock alignments. These events belong to the Amatrice earthquake's aftershocks and demonstrate the temporal and geometrical complexity of the fault system activated during the AVN sequence. Finally, the deeper focal mechanism solution, occurred two days before the Norcia mainshock, could be related to the activity of the nearby basal SZ. The role of this low–angle east–dipping SZ is still a matter of debate (Chiaraluce et al., 2017; Lavecchia et al., 2017; Vuan et al., 2017; Improta et al., 2019; Michele et al., 2020; Tan et al., 2021). However, the CMT–3D solution is not geometrically coherent with the SZ, its east–dipping fault plane dips 42°, too much for a low–angle structure.

In order to characterize the kinematic of the faults activated between the Norcia and Amatrice domain, we cross–cut the seismicity through the largest Amatrice aftershock (Figure 4d), an area marked by a high–density of CMT–3D solutions. In this section, the aftershocks delineate two opposite dipping structures that overly the sub–horizontal, gently NE–dipping SZ, here very well illuminated. Unfortunately, the moment tensor solutions located on or near this tectonic structures are not consistent to each other and don't help discriminating the kinematic behaviour of the structures. On the contrary, the NE–dipping alignment of kinematically coherent moment tensor solutions, outlined by the dashed blue line in Figure 4d, perfectly fit with the antithetic fault suggested by Scognamiglio, Tinti, and Quintiliani (2016) for the Amatrice aftershock and partially depicted by the aftershocks' location. The preferred focal plane dips $\sim 50°$. All these earthquakes are aftershocks of the Amatrice mainschock.

Moving down toward southeast through the Laga Mts. fault system, section E–E' hosts the M_w 5.96 Amatrice earthquake. Very few aftershocks imagine the mainshock's fault, however, the retrieved mainshock's moment tensor solution perfectly fits the hinted 50°SW–dipping plane, as well as the other two displayed CMT–3D solutions (Figure 5a). The lack of aftershocks in the first 7–8 km depth is consistent with the location of the main slip patches of the Amatrice finite–fault source model (Tinti et al., 2016).

South of the Amatrice ruptured area, two cross–sections (F–F' and G–G') describe the geometry and the kinematic of the faults involved in the southern termination of the AVN sequence. Section F–F' (Figure 4b) is characterized by a main SW–dipping fault compatible with the dip–slip kinematic shown by the nearby CMT–3D solutions. The shallowest focal mechanisms have a preferred nodal plain dipping between 50° and 60°, while the deepest mechanisms show dip values ranging between 30°–40°. The observed lowering dip angle seems to confirm the suggestion by Michele et al. (2020) that, in this area, shallow seismicity flattens with depth. The CMT–3D solutions, located in the small cluster of earthquakes on the fault hangingwall, helps to interpret this cluster as a minor antithetic fault. In Figure 4c, section G–G' crosses in between the four M_w 5+ Campotosto earthquakes occurred on 18

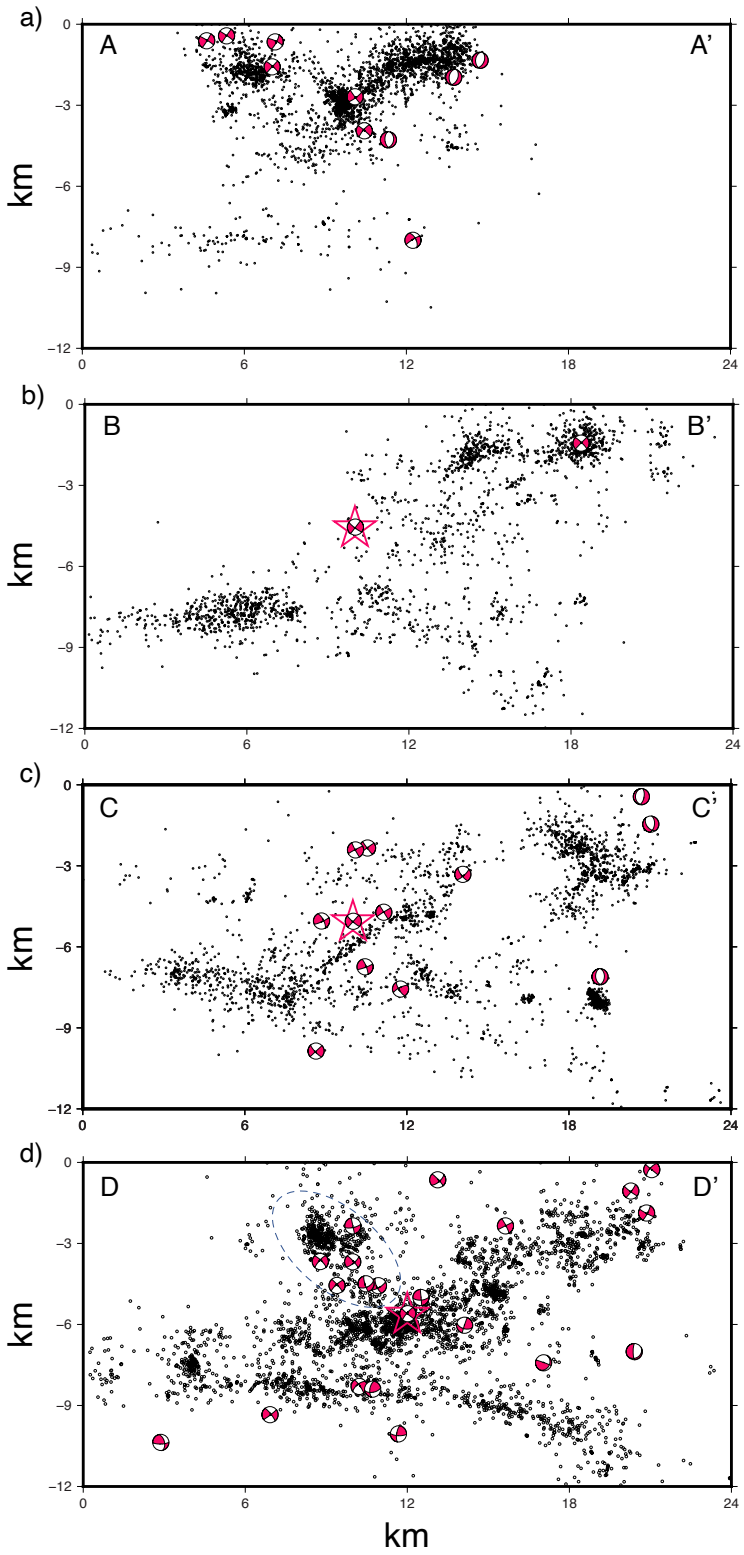

Figure 4. Cross-sections A–A' to D–D' along profiles shown in Figure 1. The cross-sections include events and focal mechanisms within ±2.0 km from each profile. Big stars enclose the focal mechanism solutions indicated by red or black stars in Figure 1.

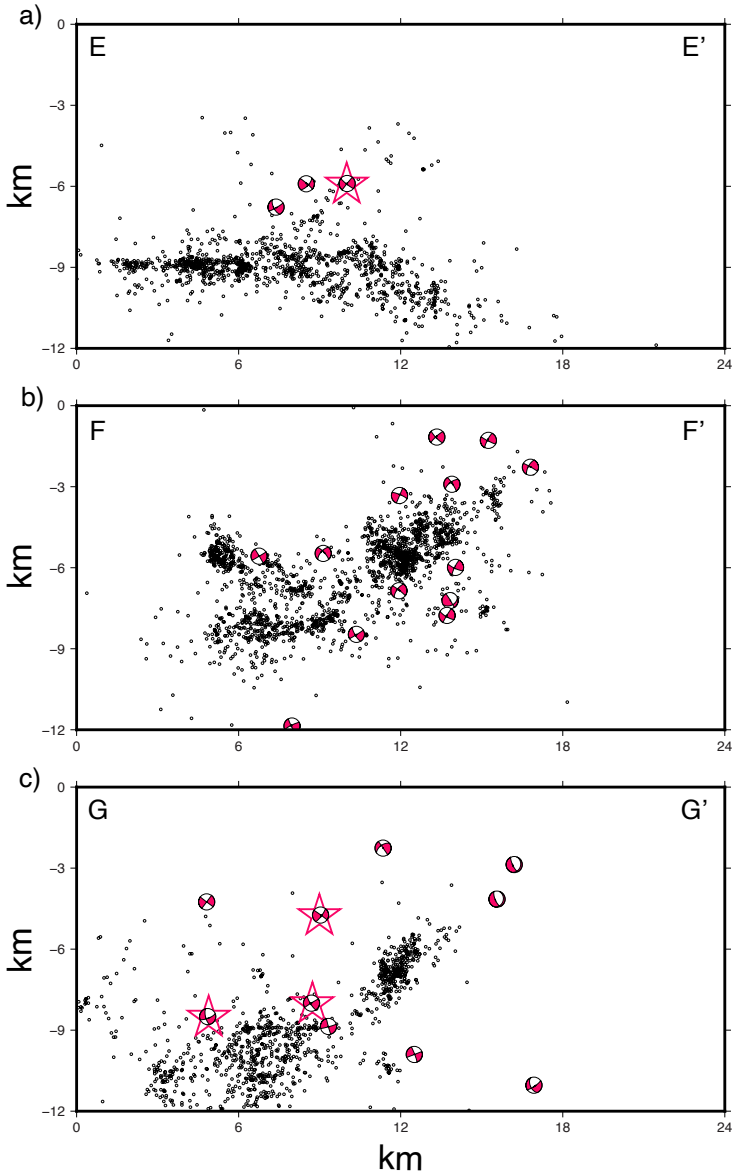

Figure 5. Same as Figure 4 but for cross–sections E–E' to G–G' along profiles shown in Figure 1.

January 2017 and includes the seismicity within 3 km from the profile. It is further clear, in this section, the kink in the activated fault structures supported by the geometry of nearby CMT–3D solutions which show a decrease of the SW–dipping angles with depth. The depth of the M_w 5.4 moment tensor solution is consistent with the finite fault model of Cheloni et al. (2019) characterized by a main slip patch located up–dip with respect to the hypocentral location.

Finally, section H–H' gives an overall view of the along–strike geometry and kinematic of the tectonic structures involved in the AVN sequence, and of the extension of the three mainshocks' rupture areas (Figure 6). Along this section, the retrieved CMT–3D solutions help in describing the rupture characteristics of the numerous activated fault segments. In particular, our moment tensor solutions well define the seismicity bounding the Amatrice rupture area and perfectly fit the southern extension of the SZ. These focal mechanisms, outlined by a black dashed line in map and in section H–H', are all characterized by a low–

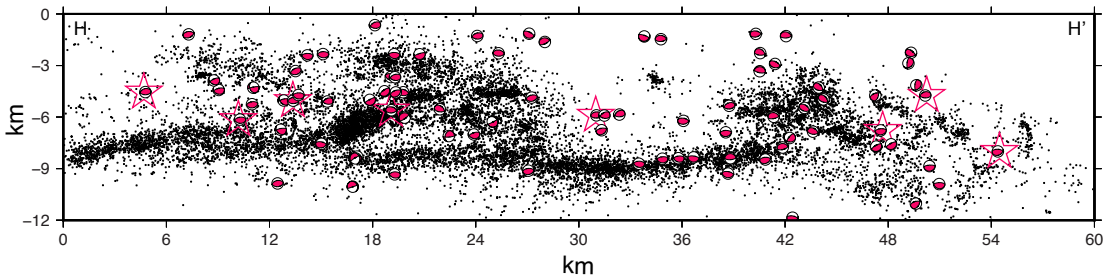

Figure 6.

Same as Figures 4,5 but for the longitudinal section H–H' shown in Figure 1.

angle SW–dipping plane and a high-angle NE–dipping plane. None of these fault planes agree with the NE–low–dipping geometry of the SZ, leaving the debate on the role of this sub-horizontal feature still open.

4 Discussion and Conclusions

We generated a new CMT catalogue for the 2016–2017 AVN sequence by inverting three–component waveforms within the recent 3D lithospheric wavespeed model for Italy *Im25*. The CMT–3D catalog contains 159 solutions with moment magnitudes ranging from 3.01 to 6.43 and depths from -0.6 km to 15.1 km (see Table S1 and the ".csv" Table in the supplementary material).

The quality of the solutions is provided by the newly developed parameter τ, which quantifies the capability of the CMT–3D solutions of modeling the real data, therefore giving a reliable estimate of the seismic source parameters. Based on τ, we found that $\sim 83\%$ of the retrieved solutions shows a good or excellent fit between data and synthetics, while $\sim 14\%$ shows a poor fit mainly caused by the small number of selected time windows due to the low event's magnitude.

The presented CMT–3D catalog contains the uncertainties on the components of the moment tensor, which translate into uncertainties on the derived parameters allowing us to perform some statistical analysis on the inverted source parameters including the seismic moment, and the time and spatial location parameters.

We compared the M_w determined in our study to that derived from the TDMT catalog, which is based on an ad–hoc 1D wavespeed model for Central Italy. Differences between the M_w estimates are subtle, with almost all the values contained in a very small interval (± 0.1). This represents a remarkable attainment being M_w the reference estimate of earthquake size. Since the use of the well–calibrated 1D or 3D wavespeed models for MT calculation in the region does not influence the M_w estimates, we can infer that the two models confirm each other. The robustness of the M_w values is further assessed by the $M_w - M_L$ regression analysed in our study, which yields values similar to those of Malagnini and Munafó (2018).

The agreement between the M_w values from the compared catalogs, TDMT and CMT–3D, as well as the kinematic consistency of the corresponding mechanisms, quantified by the Kagan angle, confirm the reliability of the retrieved solutions.

A significant enhancement of the CMT–3D MT is the inferred events' depth. Discrepancies with respect to the earthquake focal depths obtained by TDMT result from a raw exploration in depth (with a 1–km–increment) of that procedure. We can therefore assume that focal depths obtained by our technique are improved values. As a result, inversions for the location parameters, differently from the TDMT technique, give us the possibility to investigate the features and the role of the structures activated during the sequence, and to compare our location parameters with the most accurate available location catalogs.

Using a regional high–resolution 3D wavespeed model in an area where a reference well–calibrated 1D wavespeed model is available is a necessary test in order to apply the 3D procedure for areas where 1D wavespeed model is not as reliable.

The proposed CMT–3D catalog can be used in full–waveform inversion to improve the resolution of 3D Earth models, in studying the temporal and spatial variations of stress conditions, and the depth distribution of seismicity. It can also contribute to explain the complexity of the seismogenic processes active in the Central Apennines and help in comprehending the main features of the seismic sequence. The improvement of our understanding on the activated fault systems, derived by the adoption of 3D wavespeed models, could have potential implications to mitigate seismic hazard and risk in the area.

References

Barchi, M., DeFeyter, A., Magnani, B., Minelli, G., Pialli, G., & Sotera, B. (1998a). The structural style of the umbria-marche fold and thrust belt. *Memorie della Societa Geologica Italiana*, *52*, 557–578.

Barchi, M., DeFeyter, A., Magnani, B., Minelli, G., Pialli, G., & Sotera, B. (1998b). Extensional tectonics in the northern apennines (italy): Evidence from the crop03 deep seismic reflection line. *Memorie della Societa Geologica Italiana*, *52*, 528–538.

Bernardi, F., Braunmiller, J., Kradolfer, U., & Giardini, D. (2004). Automatic regional moment tensor inversion in the european-mediterranean region. *Geophysical Journal International*, *157*, 703–716.

Boncio, P., Lavecchia, G., & Pace, B. (2004). Defining a model of 3D seismogenic sources for seismic hazard assessment applications: The case of central Apennines (Italy). *Journal of Seismology*, *8*(3), 407—425.

Carminati, E., & Doglioni, C. (2012). Alps vs. Apennines: The paradigm of a tectonically asymmetric Earth. *Earth-Science Reviews*, *112*(1), 67—96.

Centamore, E., & Rossi, D. (2009). Neogene–quaternary tectonics and sedimentation in the central apennines. *Bollettino della Societa Geologica Italiana*, *128*(1), 73–88.

Cheloni, D., Falcucci, E., & Gori, S. (2019). Half-graben rupture geometry of the 30 october 2016 mw mt. vettore-mt. bove earthquake, central italy. *Geophys. Res. Lett.*, *124*(4), 4091–4118.

Chiang, A., Pitarka, A., Ford, S., Ezzedine, S., & Vorobiev, O. (2019). *3d moment tensor inversion of underground chemical explosions from the source physics experiments* (Tech. Rep.). Livermore, CA (United States): Lawrence Livermore National Lab. (LLNL).

Chiarabba, C., Jovane, L., & DiStefano, R. (2005). A new view of Italian seismicity using 20 years of instrumental recordings. *Tectonophysics*, *395*(3), 251—268.

Chiaraluce, L., Di Stefano, R., Tinti, E., Scognamiglio, L., Michele, M., Casarotti, E., ... Marzorati, S. (2017). The 2016 central italy seismic sequence: A first look at the mainshocks, aftershocks, and source models. *Seismological Research Letters*, *88*(3), 757–771.

Collins, D., Pinnock, I., Shumila, V., & Hosseini, Z. (2014). *3d velocity model with complex geology and voids for microseismic location and mechanism* (Tech. Rep.). ACG Deep Mining 2014.

Covellone, B., & Savage, K. (2012). A quantitative comparison between 1d and 3d source inversion methodologies: Application to the middle east. *Bullettin of the Seismological Society of America*, *102*(5), 2189–2199.

D'Agostino, N., Mantenuto, S., D'Anastasio, E., Avallone, A., Barchi, M., Collettini, C., ... Fastellini, G. (2009). Contemporary crustal extension in the Umbria–Marche Apennines from regional CGPS networks and comparison between geodetic and seismic deformation. *Tectonophysics*, *476*(1), 3—12.

Fichtner, A., & Simuté, S. (2018). Hamiltonian monte carlo inversion of seismic sources in complex media. *Journal of Geophysical Research: Solid Earth*, *123*, 2984–2999.

Hejrani, B., Tkalčić, H., & Fichtner, A. (2017). Centroid moment tensor catalogue using a 3-d continental scale earth model: Application to earthquakes in papua new guinea and the solomon islands. *Journal of Geophysical Research: Solid Earth*, *122*, 5517–5543.

Herrmann, R., Malagnini, L., & Munafó, I. (2011). Regional moment tensor of the 2009 l'aquila earthquake sequence. *Bullettin of the Seismological Society of America*, *101*(3), 975–993.

Hingee, M., Tkalčić, H., Fichtner, A., & Sambridge, M. (2011). Seismic moment tensor inversion using a 3–d structural model: applications for the australian region. *Geophysical Journal International*, *184*(2), 949–964.

Hjörleifsdóttir, V., & Ekström, G. (2010). Eeffects of three-dimensional earth structure on cmt earthquake parameters. *Journal Physics of the Earth and Planetary Interiors*(3–4), 178–190.

Improta, L., Latorre, D., Margheriti, L., Nardi, A., Marchetti, A., Lombardi, A., ... Moretti, M. (2019). Multi-segment rupture of the 2016 amatrice- visso-norcia seismic sequence (central italy) constrained by the first high-quality catalog of early aftershocks. *Sci. Rep.*, *9*(1), 1–13.

Jechumtálová, Z., & Bulant, P. (2013). Effects of 1–d versus 3–d velocity models on moment tensor inversion in the dobrá voda locality at the little carpathians region, slovakia. *Seismic Waves in Complex 3-D Structures, Report 23, (Department of Geophysics, Faculty of Mathematics and Physics, Charles University in Prague*, 253–269.

Kagan, Y. (1991). 3-d rotation of double-couple earthquake sources. *Geophysics Journal International*, *106*, 709–716.

La Longa, F., Crescimbene, M., & Camassi, R. (2014). *Il contrasto di voci e dicerie sui terremoti del 20 e 29 maggio 2012 in pianura padana.* 33rd Annual GNGTS symposium.

Lavecchia, G. (1985). Il sovrascorrimento dei monti sibillini: analisi cinematica e strutturale. *Bollettino della Societa Geologica Italiana*, *104*, 161–194.

Lavecchia, G., Adinolfi, G., De Nardis, M., Ferrarini, F., cirillo, D., Brozzetti, F., ... Zollo, A. (2017). Faulting model for the largest aftershock of the l'aquila 1 2009 sequence and implications for unknown active extensional sources in central italy. *Terra Nova*, *29*, 77–89.

Li, H., Chang, X., Xie, X.-B., & Wang, Y. (2021). Microseismic moment–tensor inversion and sensitivity analysis in vertically transverse isotropic media. *Geophysics*, *86*(2), KS23–KS36.

Liu, Q., Polet, J., Komatitsch, D., & Tromp, J. (2004). Spectral–element moment tensor inversions for earthquakes in southern california. *Bullettin of the Seismological Society of America*, *94*(5), 1748–1761.

Maggi, A., Tape, C., Chen, M., Chao, D., & Tromp, J. (2009). An automated time-window selection algorithm for seismic tomography. *Geophysical Journal International*, *178*(1), 257–281.

Magnoni, F., Casarotti, E., Komatitsch, D., Di Stefano, R., Ciaccio, M., Tape, C., ... Tromp, J. (2021). Adjoint tomography of the italian lithosphere. *Communications Earth and Environment*, submitted.

Malagnini, L., & Munafó, I. (2018). On the relationship between ml and mw in a broad range: An example from the apennines, italy. *Bulletin of the Seismological Society of America*, *108*(2), 1018–1024.

Michele, M., Chiaraluce, L., Di Stefano, R., & Waldhauser, F. (2020). Fine-scale structure of the 2016–2017 central italy seismic sequence from data recorded at the italian national network. *Journal of Geophysical Research: Solid Earth*, *125*, e2019JB018440.

Munafò, I., Malagnini, L., & Chiaraluce, L. (2016). On the relationship between M_w and M_L for small earthquakes. *Bull. Seismol. Soc. Am.*, *106*, 2402-–2408. doi: 10.1785/0120160130

Nayak, A., & Dreger, D. (2018). Source inversion of seismic events associated with the sinkhole at napoleonville salt dome, louisiana using a 3–d velocity model. *Geophysical Journal International*, *214*, 1808–1829.

Peter, D., Komatitsch, D., Luo, Y., Martin, R., LeGoff, N., Casarotti, E., ... Tromp, J. (2011). Forward and adjoint simulations of seismic wave propagation on fully unstructured hexahedral meshes. *Geophysical Journal International*, *186*, 721–739.

Pucci, P., S. adn De Martini, Civico, R., Villani, F., Nappi, R., & Ricci, T. e. a. (2017). Coseismic ruptures of the 24 august 2016, mw 6.0 amatrice earthquake (central italy). *Geophysical Research Letters*, *44*, 2138—2147.

Scognamiglio, L., Magnoni, F., Tinti, E., & Casarotti, E. (2016). Uncertainty estimations for moment tensor inversions: the issue of the 2012 may 20 emilia earthquake. *Geophysical Journal International*, *206*, 792–806.

Scognamiglio, L., Tinti, E., Casarotti, E., Pucci, S., Villani, F., Cocco, M., ... Dreger, D. (2018). Complex fault geometry and rupture dynamics of the mw 6.5, 30 october 2016, central italy earthquake. *Journal of Geophysical Research: Solid Earth*, *123*,

2018JB015603.

Scognamiglio, L., Tinti, E., & Michelini, A. (2009). Real-time determination of seismic moment tensor for italian region. *Bullettin of the Seismological Society of America*, *99*(4), 2223–2242.

Scognamiglio, L., Tinti, E., & Quintiliani, M. (2016). The first month of the 2016 central italy seismic sequence: fast determination of time domain moment tensors and finite fault model analysis of the ml 5.4 aftershock. *Annals of Geophysics*, *59*.

Takemura, S., Kazuo, Y., & Shiomi, K. (2021). ong-period ground motion simulation using centroid moment tensor inversion solutions based on the regional three-dimensional model in the kanto region, japan. *Earth, Planets and Space*, *73*(15).

Takemura, S., Kimura, T., Saito, T., Kubo, H., & Shiomi, K. (2018). Moment tensor inversion of the 2016 southeast offshore mie earthquake in the tonankai region using a three-dimensional velocity structure model: effects of the accretionary prism and subducting oceanic plate. *Earth, Planets and Space*, *70*(50).

Takemura, S., Okuwaki, R., Kubota, T., Shiomi, K., Kimura, T., & Noda, A. (2020). Centroid moment tensor inversions of offshore earthquakes using a three-dimensional velocity structure model: slip distributions on the plate boundary along the nankai trough. *Geophysical Journal International*, *222*, 1109–1125.

Tan, Y., Waldhauser, F., Ellsworth, W., Zhang, M., Zhu, W., Michele, M., ... Segou, M. (2021). Machine–learning–based high–resolution earthquake catalog reveals how complex fault structures were activated during the 2016–2017 central italy sequence. *The Seismic Record*, *1*(1), 11–19, doi: 10.1785/0320210001.

Tinti, E., Scognamiglio, L., Michelini, A., & Cocco, M. (2016). Slip heterogeneity and directivity of the ml 6.0, 2016, amatrice earthquake estimated with rapid finite-fault inversion. *Geophys. Res. Lett.*, *43*(20), 10,745–10,752.

Vuan, A., Sugan, L., M.and Chiaraluce, & Di Stefano, R. (2017). Loading rate variations along a midcrustal shear zone preceding the mw 6.0 earthquake of 24 august 2016 in central italy. *Geophysical Research Letters*, *44*, 12,170–12,180.

Walters, R., Gregory, L., Wedmore, L., Craig, T., McCaffrey, K., Wilkinson, M., ... Goodall, H. e. a. (2018). Dual control of fault intersections on stop–start rupture in the 2016 central italy seismic sequence. *Earth Planet. Sci. Lett.*, *500*, 1–14.

Wang, X., & Zhan, Z. (2019). Moving from 1–d to 3–d velocity model: automated waveform–based earthquake moment tensor inversion in the los angeles region. *Geophysical Journal International*, *220*(1), 218–234.

Wang, X., & Zhan, Z. (2020). Seismotectonics and fault geometries of the 2019 ridgecrest sequence: Insight from aftershock moment tensor catalog using 3-d green's functions. *Journal of Geophysical Research: Solid Earth*, *124*, e2020JB019577.

Willacy, C., van Dedem1, E., Minisini, S., Li, J., Blokland, J., Das, I., & Droujinine, A. (2019). Full–waveform event location and moment tensor inversion for induced seismicity. *Geophysics*, *84*(2), KS39–KS57.

Yang, W., Hauksson, E., & Shearer, P. (2012). Computing a large refined catalog of focal mechanisms for southern california (1981–2010): Temporal stability of the style of faulting. *Bullettin of the Seismological Society of America*, *102*(3), 1179–1194.

Zhu, L., & Zhou, X. (2016). Seismic moment tensor inversion using 3d velocity model and its application to the 2013 lushan earthquake sequence. *Physics and Chemistry of the Earth*, *95*, 10–18.

Supporting Information for Centroid Moment Tensor catalog with 3D lithospheric wavespeed model: the 2016–2017 Central Apennines sequence

P. Artale Harris[1], L. Scognamiglio[1], F. Magnoni[1], E. Casarotti[1]and E. Tinti[1,2]

[1]Istituto Nazionale di Geofisica e Vulcanologia, Roma

[2]Sapienza Universitá di Roma

Contents of this file

Introduction The Auxiliary Material contains text S1, Figures (S1–S3), one Table (S1) and one large comprehensive Table (S1, in .csv extension) relative to specific information about the source modeling and the stability check of the results reported in the principal text.

Text S1. Using the source inversion code 'pycmt3d' it is possible to perform an additional bootstrap analysis which randomly considers multiple subsets of time windows among the

selected dataset and provides an ensemble of the corresponding source solutions. This procedure allows us to obtain some statistic estimates on the source inversion results, such as calculation of mean value and standard deviation for the inverted moment tensor components and earthquake location (longitude, latitude and depth). The uncertainties shown in Figures 3b,c come from the pycmt3d bootstrap analysis and are propagated using the python package 'uncertainties' (`https://pythonhosted.org/uncertainties/`).

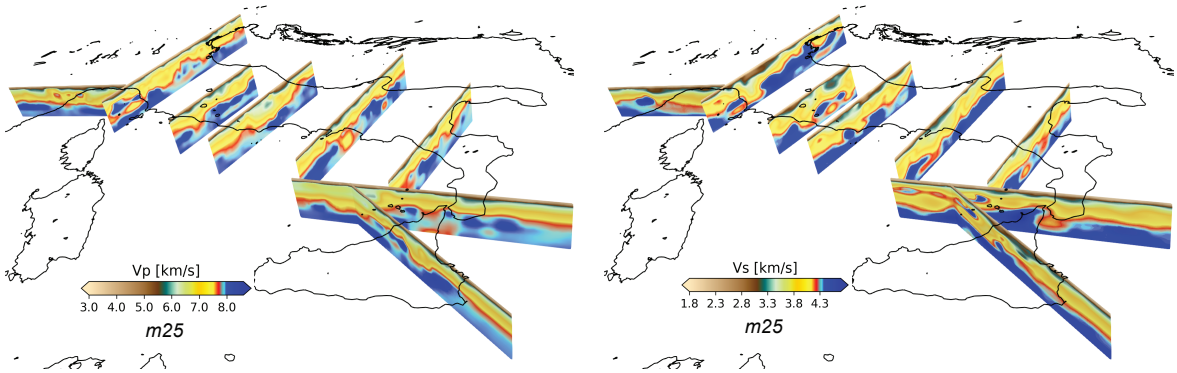

Figure S1. The 3D lithospheric wavespeed model for Italy *Imagine25* (Magnoni et al., 2021).

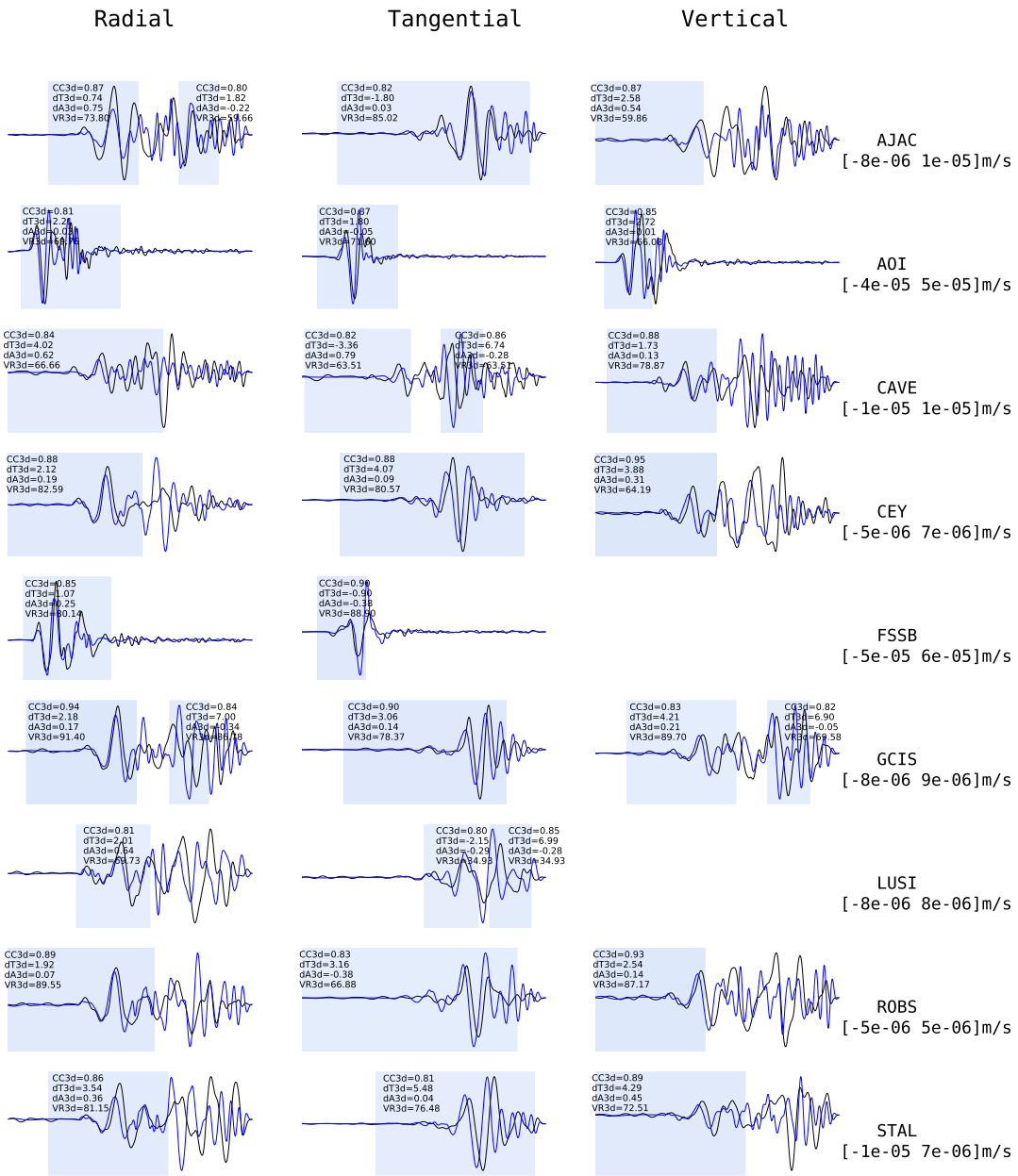

Figure S2. An example of fit from a set of stations for the event n. 2 in Table S1. Black lines represent data and blue lines are the synthetics. The blue squares are the selected time windows, containing the FLEXWIN parameteres. If seismograms are not present that means that there are no selected windows. The numbers in brackets represent the amplitude range of the plot in m/s for each station.

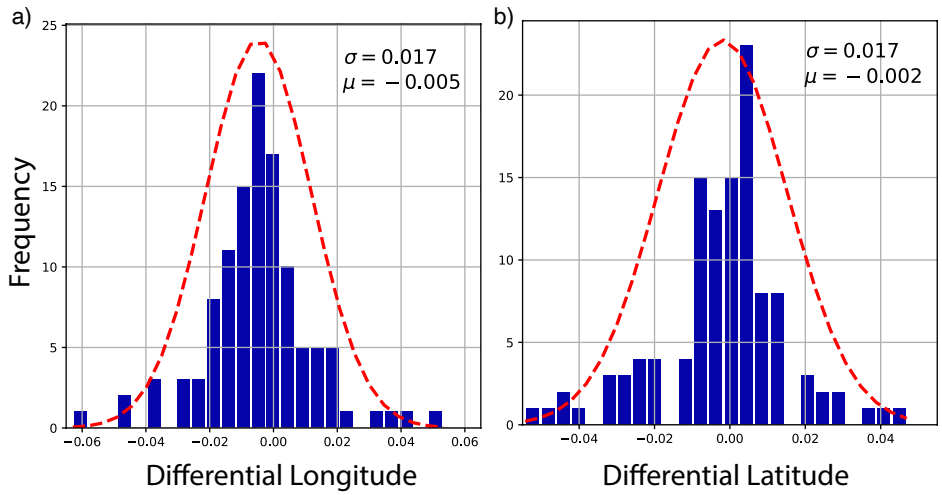

Figure S3. Histograms of differential longitude and latitude for a subset of coinciding events beetween Michele et al. (2020) and CMT–3D (this study). A normal fit is superimposed.

Table S1: Source solution parameters for each analysed event. Latitude, Longitude and Depth are the centroid localization parameters; $s_i/d_i/r_i$ are the strike/dip/rake values for the two planes; KA stands for Kagan Angle.

Id	Origin Time	Lat	Lon	Dep	s1	d1	r1	s2	d2	r2	M_w	KA	τ
1	2016/08/24-01:36:32	42.7058	13.2474	5.90	326	39	-97	157	51	-83	5.96	5.70	0.32
2	2016/08/24-02:33:29	42.7959	13.1678	5.60	325	40	-85	140	49	-93	5.28	4.53	0.26
3	2016/08/24-03:08:10	42.6385	13.2734	6.89	327	62	-93	155	27	-83	3.77	7.67	0.42
4	2016/08/24-03:17:59	42.7720	13.1617	5.36	350	65	-99	192	26	-70	3.66	5.06	3.36
5	2016/08/24-03:40:11	42.6251	13.2454	9.29	131	31	-108	332	60	-79	4.08	9.90	0.29
6	2016/08/24-04:06:50	42.7815	13.1334	3.67	348	46	-65	135	49	-113	4.33	12.55	0.25
7	2016/08/24-04:25:58	42.6513	13.2363	8.39	348	59	-89	167	30	-91	3.48	6.00	0.37
8	2016/08/24-04:33:09	42.6444	13.2272	6.22	325	50	-86	140	39	-93	3.39	6.12	0.37
9	2016/08/24-04:38:09	42.6304	13.2357	6.75	183	35	-54	322	62	-112	3.35	16.77	7.9
10	2016/08/24-04:44:38	42.7547	13.1905	6.08	301	41	-117	155	54	-67	3.49	4.00	7.81
11	2016/08/24-04:57:37	42.8439	13.0558	-0.24	312	43	-76	114	48	-101	3.55	7.43	8.87
12	2016/08/24-05:31:31	42.6760	13.2105	5.85	329	33	-115	179	60	-73	3.28	7.89	0.33
13	2016/08/24-05:36:18	42.8079	13.1652	5.00	332	85	-117	233	28	-10	3.30	7.29	0.38
14	2016/08/24-06:54:54	42.7920	13.1490	4.50	209	40	-26	320	72	-127	3.19	15.37	0.4
15	2016/08/24-09:31:43	42.8195	13.1771	14.12	324	68	-177	233	88	-21	3.43	4.35	0.34
16	2016/08/24-11:50:30	42.8332	13.1558	7.56	129	31	-100	322	59	-83	4.52	3.74	0.29
17	2016/08/24-14:02:20	42.8021	13.2530	2.04	334	54	-133	213	53	-46	3.63	7.58	0.36
18	2016/08/24-17:46:09	42.6716	13.2276	8.71	345	55	-84	155	35	-98	4.20	6.10	0.25
19	2016/08/24-20:21:35	42.7890	13.1579	4.57	183	35	-42	311	66	-117	3.22	12.34	0.36
20	2016/08/24-23:22:05	42.6521	13.2155	8.42	164	28	-81	334	61	-94	4.00	4.27	0.33
21	2016/08/25-03:17:16	42.7638	13.2096	7.01	342	62	-103	189	30	-66	4.28	3.76	0.28
22	2016/08/25-04:12:11	42.6951	13.2337	5.91	345	41	-106	187	50	-75	3.17	7.63	0.37
23	2016/08/25-04:51:40	42.6279	13.3338	1.29	321	27	-89	141	62	-90	3.73	3.46	0.35
24	2016/08/25-12:36:05	42.5943	13.3083	4.97	352	43	-40	113	63	-126	4.38	16.14	0.28
25	2016/08/25-19:40:44	42.5919	13.2759	5.47	349	49	-52	120	52	-125	3.42	9.54	0.39
26	2016/08/26-00:04:09	42.6819	13.2830	1.47	144	57	-89	323	32	-91	3.49	8.84	0.33
27	2016/08/26-04:28:25	42.5988	13.3121	4.28	111	63	-125	349	42	-40	4.69	20.18	0.24
28	2016/08/26-05:17:05	42.7546	13.2148	6.26	134	74	114	254	28	32	3.27	17.47	0.45
29	2016/08/26-05:32:52	42.7739	13.1564	2.35	332	78	-107	210	20	-33	3.31	18.97	0.37
30	2016/08/26-16:05:29	42.7019	13.1455	7.63	312	64	-96	146	26	-76	3.48	7.50	0.35

Table S1 continued from previous page

31	2016/08/27-01:26:39	42.8446	13.2461	1.06	159	54	-79	322	36	-104	3.73	3.00	0.37
32	2016/08/27-02:50:59	42.8531	13.2477	1.87	161	63	-80	319	28	-108	3.89	11.37	0.24
33	2016/08/27-06:20:30	42.5483	13.3246	2.26	332	55	-57	104	46	-128	3.28	9.75	0.36
34	2016/08/27-10:40:14	42.8607	13.2539	-0.56	162	64	-74	310	29	-118	3.52	14.17	0.37
35	2016/08/28-06:37:19	42.7309	13.2098	9.12	323	58	-99	161	33	-74	3.34	4.66	0.35
36	2016/08/28-13:07:32	42.6250	13.2897	3.33	151	67	-101	358	25	-64	3.53	7.59	0.36
37	2016/08/28-15:37:38	42.7713	13.1151	9.34	158	38	-95	345	51	-85	3.50	5.44	0.35
38	2016/08/28-15:55:35	42.7976	13.2461	6.20	42	30	-96	229	59	-86	4.06	22.82	0.27
39	2016/08/28-16:42:01	42.8267	13.1431	2.34	155	37	-91	337	52	-88	3.68	2.50	0.35
40	2016/08/29-01:44:25	42.7733	13.1838	5.54	338	40	-58	119	56	-114	3.27	10.58	0.35
41	2016/08/30-00:35:55	42.8032	13.1365	8.30	343	56	-58	115	44	-128	3.35	7.64	0.32
42	2016/08/31-11:26:01	42.8418	13.1434	4.72	341	58	-87	156	31	-94	3.86	6.77	0.38
43	2016/08/31-11:52:31	42.8738	13.2517	0.44	279	89	-171	189	81	0	3.31	6.42	0.37
44	2016/08/31-13:23:04	42.7683	13.2478	4.91	155	70	-72	292	25	-129	3.33	7.00	0.36
45	2016/08/31-18:12:52	42.8324	13.2576	7.01	229	71	0	139	89	161	3.46	8.13	0.37
46	2016/09/01-03:53:03	42.6280	13.3166	5.99	141	64	-83	308	26	-102	3.58	9.11	0.39
47	2016/09/01-11:35:57	42.5708	13.3267	4.74	183	36	-15	286	80	-125	3.27	3.99	0.42
48	2016/09/03-01:34:12	42.7850	13.1476	3.68	341	48	-99	175	42	-79	4.16	6.06	0.25
49	2016/09/03-10:18:51	42.8849	13.2262	7.11	296	84	-177	205	87	-5	4.28	7.26	0.25
50	2016/09/07-18:13:26	42.8407	13.2602	0.27	124	53	-106	330	39	-69	3.23	13.09	0.4
51	2016/09/15-14:40:52	42.7873	13.1450	-0.31	201	33	-50	336	65	-112	3.60	18.83	0.34
52	2016/09/19-23:34:25	42.6910	13.2806	1.31	322	71	-74	101	24	-128	3.65	25.08	0.34
53	2016/09/20-01:20:53	42.6873	13.2914	6.02	317	83	-59	58	30	-166	3.27	11.25	7.08
54	2016/09/22-20:03:54	42.7204	13.1865	1.15	104	34	-136	335	67	-64	3.33	11.30	0.4
55	2016/09/30-19:22:28	42.8748	13.2558	1.46	291	63	-174	198	85	-26	3.25	47.23	0.31
56	2016/09/30-19:38:37	42.8722	13.2562	2.03	141	55	-112	357	40	-61	3.47	43.80	0.34
57	2016/10/02-23:47:07	42.8174	13.2483	-4.57	44	47	85	230	43	94	3.17	112.96	6.18
58	2016/10/04-12:41:35	42.8637	13.1142	7.25	347	54	-43	106	55	-135	3.49	2.76	6.35
59	2016/10/08-12:19:03	42.7787	13.1444	4.56	339	49	-73	134	43	-108	3.54	9.92	0.36
60	2016/10/08-18:11:09	42.7427	13.1954	2.29	332	42	-84	145	47	-94	3.89	9.76	0.36
61	2016/10/16-09:32:35	42.7625	13.2113	1.28	334	46	-101	171	44	-77	3.93	9.58	0.24
62	2016/10/26-17:10:36	42.8774	13.1437	6.15	337	54	-94	165	36	-83	5.32	4.13	0.23
63	2016/10/26-19:18:08	42.9180	13.1045	4.55	166	53	-81	331	37	-101	5.86	8.57	0.29

Table S1 continued from previous page

64	2016/10/26-21:42:01	42.8676	13.1380	5.25	328	55	-100	166	35	-75	4.45	8.02	0.23
65	2016/10/27-03:19:27	42.8567	13.1741	3.32	321	54	-117	183	43	-57	3.93	22.14	0.27
66	2016/10/27-03:50:24	43.0139	13.1126	8.00	137	33	-132	5	66	-65	4.09	13.23	0.26
67	2016/10/27-08:21:45	42.8803	13.1204	4.42	184	27	-70	343	63	-99	4.31	7.25	0.25
68	2016/10/27-17:22:23	42.8385	13.1150	5.04	3	64	-89	182	25	-91	4.23	2.34	0.27
69	2016/10/29-16:24:33	42.8406	13.1113	9.86	325	48	-101	162	42	-77	4.11	6.31	0.25
70	2016/10/30-06:40:17	42.8392	13.1300	5.05	329	42	-99	161	47	-81	6.43	8.06	0.32
71	2016/10/30-10:19:26	42.8488	13.1549	4.24	37	41	-1	129	88	-131	3.78	36.38	8.0
72	2016/10/30-10:50:37	42.8443	13.0857	4.29	200	14	-75	6	75	-93	3.69	15.20	0.37
73	2016/10/30-11:21:08	43.0572	13.0943	7.92	157	58	-64	294	39	-125	3.92	9.83	0.26
74	2016/10/30-11:58:17	42.8316	13.0603	15.45	337	82	-85	128	8	-118	4.07	6.11	0.23
75	2016/10/30-12:07:00	42.8509	13.0876	12.20	335	67	-91	159	22	-85	4.45	9.22	0.26
76	2016/10/30-13:34:54	42.7994	13.1948	6.03	149	72	-55	263	38	-150	4.07	3.62	0.24
77	2016/10/30-14:24:44	42.7610	13.0660	10.37	236	16	-45	10	78	-101	3.39	11.63	0.36
78	2016/10/30-18:21:09	42.8084	13.1736	0.65	339	47	-106	182	45	-73	3.88	9.59	0.27
79	2016/10/31-03:27:40	42.7653	13.0982	13.40	349	81	-101	222	14	-37	4.02	12.71	0.23
80	2016/10/31-07:05:44	42.8474	13.1315	6.74	354	69	-92	182	20	-82	3.99	5.67	0.24
81	2016/10/31-08:40:35	42.8325	13.1344	2.41	337	62	-88	154	27	-92	3.36	5.73	0.37
82	2016/11/01-07:56:39	43.0220	13.1566	4.89	322	42	-109	167	50	-73	4.76	8.30	0.23
83	2016/11/02-19:37:49	42.8799	13.0771	1.19	310	51	-108	158	41	-68	3.61	13.85	0.37
84	2016/11/03-00:35:01	43.0243	13.0590	6.25	171	22	-68	329	68	-98	4.68	4.24	0.25
85	2016/11/03-10:14:13	42.8110	13.2070	2.35	337	63	-87	153	26	-94	2.96	32.15	0.36
86	2016/11/05-11:05:45	42.9816	13.1956	-0.20	307	17	-106	144	73	-85	3.45	31.17	0.37
87	2016/11/07-18:56:16	42.8896	13.1524	9.37	325	58	-107	176	35	-63	3.85	1.31	0.34
88	2016/11/12-14:43:33	42.7359	13.2263	4.87	168	39	-68	320	53	-107	4.07	10.09	0.23
89	2016/11/12-22:32:23	42.8247	13.1446	5.09	179	50	-82	348	39	-98	3.44	1.86	0.37
90	2016/11/16-11:52:22	42.8062	13.1413	8.40	223	32	-166	121	82	-57	3.81	14.69	0.37
91	2016/11/27-21:41:14	43.0220	13.0805	3.95	338	41	-73	136	50	-103	3.81	11.91	0.37
92	2016/11/29-16:14:02	42.5308	13.3099	8.86	166	16	-73	329	74	-94	4.40	8.31	0.27
93	2016/12/01-11:30:53	43.0047	13.0895	2.69	168	38	-74	328	52	-101	3.86	6.35	0.39
94	2017/01/02-03:36:13	42.8149	12.7604	4.05	162	83	19	70	70	173	3.90	10.44	0.43
95	2017/01/18-09:25:40	42.5473	13.2796	6.78	161	26	-77	327	64	-96	5.13	6.94	0.25
96	2017/01/18-10:14:09	42.5314	13.3053	4.74	334	36	-99	166	53	-82	5.46	4.42	0.25

Table S1 continued from previous page

97	2017/01/18-10:25:23	42.4970	13.3276	8.00	146	32	-82	317	57	-94	5.35	4.57	0.29
98	2017/01/18-11:07:37	42.6152	13.2749	8.47	156	32	-72	315	59	-100	4.09	7.56	0.29
99	2017/01/18-13:33:36	42.4792	13.2874	8.50	191	27	-31	309	76	-113	5.00	4.98	0.27
100	2017/01/18-15:16:10	42.6007	13.3085	6.85	339	38	-63	127	56	-109	4.30	4.52	0.24
101	2017/01/18-19:32:31	42.5921	13.2595	11.86	131	28	-101	324	62	-83	4.23	9.97	0.26
102	2017/01/19-10:25:50	42.6535	13.2454	7.61	299	54	-108	148	39	-66	3.39	18.35	8.77
103	2017/01/21-03:54:24	42.6038	13.3526	3.13	25	64	-23	125	68	-152	3.23	4.84	18.08
104	2017/01/21-09:35:55	42.7249	13.2191	1.63	150	61	-66	287	36	-126	3.68	15.84	0.37
105	2017/01/27-14:20:15	42.5407	13.3468	9.90	336	69	-89	155	20	-91	3.43	12.37	0.39
106	2017/01/28-16:14:40	42.6268	13.3156	2.91	340	57	-62	115	41	-126	3.25	11.59	0.43
107	2017/01/29-05:10:54	42.6330	13.3029	1.16	317	47	-92	140	42	-87	3.82	12.40	0.38
108	2017/02/03-03:47:55	42.9915	13.0219	0.61	155	58	-94	343	31	-82	3.86	8.23	0.3
109	2017/02/03-04:10:05	42.9918	13.0321	0.43	337	35	-84	151	54	-93	4.09	4.76	0.31
110	2017/02/03-05:40:34	43.0035	13.0468	1.58	342	43	-81	151	47	-97	3.81	5.18	0.36
111	2017/02/03-23:37:43	42.6225	13.3165	7.77	148	59	-78	306	32	-108	3.51	13.81	0.75
112	2017/02/04-02:39:13	42.9846	13.0380	-0.12	315	50	-124	182	50	-55	3.27	41.28	7.1
113	2017/02/04-03:41:58	42.9895	13.0484	-0.58	143	51	-98	338	38	-78	3.37	11.05	0.34
114	2017/02/06-23:38:56	42.9804	13.0370	1.08	313	40	-123	174	57	-64	3.55	15.96	6.62
115	2017/02/09-09:58:27	42.6637	12.6887	1.62	273	47	-92	97	42	-87	3.68	7.79	0.36
116	2017/02/09-14:14:41	42.6806	12.6858	1.43	252	47	-98	84	43	-81	3.25	5.10	7.43
117	2017/02/14-08:28:04	42.6913	13.2210	6.77	310	65	-109	170	31	-54	3.59	1.61	0.38
118	2017/02/20-03:13:30	42.5038	13.2676	4.25	330	37	-91	152	52	-88	3.89	6.01	0.38
119	2017/02/23-03:17:31	42.6019	13.2346	5.57	332	59	-91	154	30	-88	3.45	9.72	0.38
120	2017/03/20-05:02:41	42.5714	13.3748	2.87	314	65	-173	221	84	-24	3.42	25.58	0.42
121	2017/04/11-14:35:23	43.0176	13.0967	4.28	296	86	-174	206	84	-3	3.50	8.96	0.4
122	2017/04/11-14:45:26	43.0208	13.1424	1.34	195	73	2	104	87	163	3.24	21.10	0.36
123	2017/04/11-17:04:56	43.0183	13.1305	1.97	195	73	4	104	85	163	3.49	20.37	0.43
124	2017/04/11-17:25:21	43.0326	13.1318	4.51	31	88	9	301	80	178	3.31	9.35	7.8
125	2017/04/23-05:38:58	42.5649	13.3710	4.15	310	68	-174	218	85	-21	3.35	19.56	0.47
126	2017/04/27-21:16:58	42.9771	13.0579	0.85	8	35	-68	162	57	-104	3.88	11.57	0.3
127	2017/04/27-21:19:42	42.9872	13.0614	0.66	356	28	-79	165	62	-95	3.84	14.10	0.27
128	2017/05/19-04:46:53	42.7821	13.2169	7.11	313	14	-140	185	80	-78	3.25	5.17	0.4
129	2017/05/26-07:57:03	42.7765	13.2212	3.49	313	81	-92	150	8	-73	3.01	22.80	7.76

Table S1 continued from previous page

130	2017/06/02-00:21:46	42.8072	13.2300	7.42	218	79	-73	339	20	-146	3.44	4.05	0.38
131	2017/06/24-08:30:04	42.8819	13.1175	3.87	202	32	-64	352	61	-105	3.34	7.27	0.39
132	2017/06/29-21:41:21	42.6340	13.2175	8.35	130	22	-109	331	69	-82	3.55	6.12	0.36
133	2017/06/30-00:25:17	42.6304	13.2122	6.05	188	21	-46	323	74	-104	3.80	7.72	0.41
134	2017/07/01-19:17:25	42.6509	13.3088	8.39	149	68	-87	323	21	-96	3.56	5.61	0.34
135	2017/07/02-19:21:21	42.8676	13.1751	1.81	346	72	54	234	39	151	3.12	61.48	9.17
136	2017/07/22-02:13:07	42.5713	13.3852	11.04	171	36	-36	292	68	-120	4.06	5.03	0.26
137	2017/08/25-15:32:19	43.1267	13.1937	1.94	27	48	-16	128	78	-137	3.33	20.49	7.95
138	2017/09/01-10:29:31	43.0053	13.0073	7.89	267	83	-173	176	83	-6	3.26	7.99	7.71
139	2017/09/04-18:54:02	42.5640	13.3333	7.59	211	31	-23	321	78	-119	3.31	7.68	0.47
140	2017/09/05-04:34:21	42.5813	13.3525	7.72	207	35	-32	324	71	-121	3.76	5.94	0.42
141	2017/10/19-05:34:54	42.8574	13.2418	2.72	186	20	116	338	71	80	3.22	25.93	7.94
142	2017/10/20-16:16:37	42.8118	13.1503	10.05	249	19	-153	134	81	-72	3.24	5.82	0.36
143	2017/11/02-18:04:14	42.6720	13.1530	11.86	129	87	172	219	82	3	3.50	87.41	8.37
144	2017/12/03-23:34:11	42.6467	13.3410	2.28	126	64	-105	338	29	-61	4.03	11.43	0.29
145	2018/01/11-03:48:02	42.6527	13.3113	5.35	325	45	-109	172	47	-71	3.45	22.57	0.73
146	2018/02/04-12:45:33	42.6633	13.3016	8.40	316	68	-98	158	23	-68	3.17	18.78	8.24
147	2018/03/08-22:48:46	43.0773	13.0369	6.38	305	49	-115	161	46	-63	3.47	7.79	0.44
148	2018/03/08-23:32:18	43.0790	13.0302	7.78	279	80	-157	184	67	-10	3.23	41.95	0.37
149	2018/03/26-22:43:07	43.0579	12.9057	1.38	336	49	-30	87	67	-135	3.16	16.84	3.41
150	2018/04/04-02:19:45	43.0936	13.0390	4.10	305	45	-129	175	56	-56	3.97	19.78	0.24
151	2018/04/04-18:41:28	43.0769	13.0308	6.95	328	43	-107	171	48	-74	3.70	11.30	0.37
152	2018/04/10-03:11:30	43.0818	13.0254	6.29	148	61	-73	297	32	-116	4.53	8.03	0.23
153	2018/04/11-00:00:51	43.0683	13.0334	4.13	197	83	-19	289	70	-172	3.27	32.28	0.74
154	2018/04/12-13:24:03	43.0722	13.0566	7.14	263	65	-163	165	74	-25	3.42	9.99	0.34
155	2018/04/25-01:08:16	43.0720	13.0368	7.92	281	51	-139	163	59	-45	3.47	18.44	0.67
156	2018/05/21-08:49:26	43.0955	13.0208	8.84	320	34	-112	166	58	-75	3.94	7.28	0.39
157	2018/05/21-12:38:35	42.6198	13.3202	7.22	335	59	-137	220	53	-38	3.34	11.51	0.38
158	2018/07/21-08:01:50	43.0860	13.0213	9.63	304	54	-135	185	55	-45	3.21	27.29	6.61
159	2018/09/11-21:57:13	42.9451	13.2005	1.44	357	45	-81	165	44	-98	3.32	8.42	0.39